CFD Analysis of Hydrodynamics and Mass Transfer of a Gas-Liquid Bubble Column

A Project submitted to the
National Institute of Technology, Rourkela

In partial fulfillment of the requirements
of the degree of
Bachelor of Technology (Chemical Engineering)

By

Vinay Mahajan
Roll No. 10600026

Under the guidance of
Dr. H. M. Jena

DEPARTMENT OF CHEMICAL ENGINEERING
NATIONAL INSTITUTE OF TECHNOLOGY, ROURKELA
ORISSA -769 008, INDIA

2010

DEPARTMENT OF CHEMICAL ENGINEERING
NATIONAL INSTITUTE OF TECHNOLOGY,
ROURKELA -769 008, INDIA

CERTIFICATE

This is to certify that the thesis entitled "**CFD analysis of hydrodynamics and mass transfer of a gas-liquid bubble column",** submitted by **Vinay Mahajan (10600026)** to National Institute of Technology, Rourkela is a record of bonafide project work under my supervision and is worthy for the partial fulfillment of the degree of Bachelor of Technology (Chemical Engineering) of the Institute. The candidate has fulfilled all prescribed requirements and the thesis, which is based on candidate's own work, has not been submitted elsewhere.

Supervisor
Dr. H. M. Jena
Department of Chemical Engineering
National Institute of Technology
Rourkela - 769008
INDIA

ACKNOWLEDGEMENT

With a feeling of great pleasure, I express my sincere gratitude to **Prof. H. M. Jena** for his superb guidance, support and constructive criticism, which led to the improvements and completion of this project work.

I am thankful to **Prof. R. K. Singh** for acting as project coordinator.

I am also grateful to **Prof. S. K. Agarwal**, Head of the Department, Chemical Engineering for providing the necessary facilities for the completion of this project.

Vinay Mahajan (Roll No.10600026)
4th year
B. Tech.
Department of Chemical Engineering
National Institute of Technology, Rourkela

ABSTRACT

Bubble columns are widely used as gas–liquid contactors and as reactors in chemical, petrochemical and biochemical industries. Effective mixing as well as high interfacial area between the phases, leading to improved heat and mass transfer characteristics, relatively cheap to install and the lack of moving parts, are the factors that render under bubble columns an attractive choice as reactors for the described processes.

Gas-liquid flow in bubble column reactors is characterized by a combination of inherently unsteady complex processes with widely varying spatial and temporal scales. Understanding the complexity of the fluid dynamics and mass transfer in bubble column and is important due to its application in the chemical and bioprocess industries. The potential of Computational Fluid Dynamics (CFD) for describing the hydrodynamics and heat and mass transfer of bubble columns has been established by several publications in the past. CFD predicts what happens quantitatively, when fluids flow, often with the complications of simultaneous flow of heat, mass transfer (eg perspiration, dissolution), phase change (eg melting, freezing, boiling), chemical reaction (eg combustion, rusting), mechanical movement (eg of pistons, fans, rudders), stresses in and displacement of immersed or surrounding solids. Thus CFD can successfully be used to study the gas-liquid mass transfer in bubble column reactor.

In the present work an attempt has been made to understand the hydrodynamic behavior and gas-liquid mass transfer (transfer of oxygen from air to de-aerated water) of a concurrent gas(air)-liquid(water) up-flow bubble column by CFD analysis. The system used in the study is a cylindrical column of 10 cm ID and 1.88 m height. GAMBIT 2.3.16 has been used to generate a 2D coarse grid of 0.01m by 0.01m mesh size. The eulerian-eulerian approach has been used for modeling the multiphase flow and the oxygen mass transfer from air to de-aerated water and the column hydrodynamics. The standard k-ε mixture turbulence model has been used to account the effect of turbulence. FLUENT 6.3.26 has been used to simulate the system for various hydrodynamics parameters such as phase dynamics, phase velocity profile, pressure drop and the gas-liquid mass transfer. The simulated results have been compared with the experimental results found in the literature.

Keywords: Gas-liquid bubble column, mass transfer, hydrodynamics, CFD, eulerian-eulerian.

CONTENTS

CERTIFICATE		ii
ACKNOWLEDGEMENT		iii
ABSTRACT		iv
CONTENTS		v
LIST OF FIGURES		vii
LIST OF TABLES		ix
NOMENCLATURE		x
CHAPTER 1	**INTRODUCTION AND LITERATURE REVIEW**	**1-12**
1.1	Introduction	1
1.2	Bubble column reactors	2
1.3	Applications of gas-liquid bubble column	4
1.4	Mass transfer across gas-liquid interface	5
1.5	Mass transfer phenomenon studied in gas-liquid bubble column	9
1.6	Recent applications of CFD in modeling hydrodynamics and mass transfer	10
CHAPTER 2	**CFD IN MULTIPHASE MODELING**	**13-18**
2.1	Computational Fluid Dynamics	13
2.2	Advantages of CFD	13
2.3	CFD modeling of multiphase systems	14
2.4	Approaches for numerical calculations of multiphase flows	14
2.4.1	The Euler-Lagrange approach	14
2.4.2	The Euler-Euler approach	15
2.4.2.1	The VOF Model	15
2.4.2.2	The Mixture Model	15

2.4.2.3	The Eulerian Model	16
2.5	Choosing a multiphase model	16
CHAPTER 3	**CFD SIMULATION OF HYDRODYNAMICS AND GAS LIQUID MASS TRANSFER**	**19-27**
3.1	Computational Flow Model	19
3.1.1	Turbulence modeling	20
3.1.2	Modeling Species Transport	21
3.2	Problem description	22
3.3	Numerical Methodology	23
3.3.1	Geometry and Mesh	25
3.3.2	Selection of models for simulation	25
3.3.3	Solution	26
CHAPTER 4	**RESULTS AND DISCUSSION**	**28-37**
4.1	Phase Dynamics	28
4.2	Liquid and gas velocities	31
4.3	Pressure Drop	34
4.4	Gas-liquid mass transfer	35
CHAPTER 5	**CONCLUSION**	**38**
REFERENCES		**39-41**

LIST OF FIGURES

FIGURE NO.	DESCRIPTION	PAGE NO.
Figure 1.1.	The flow regime observed in gas-liquid bubble column reactors.	3
Figure 1.2.	Interphase gas liquid mass transfer.	6
Figure 2.1.	Multi-level modeling concept for fundamental hydrodynamic models of gas-liquid flow in bubble columns.	17
Figure 3.1.	Flowchart showing the general procedure for the simulation using Fluent.	24
Figure 3.2.	Coarse mesh and fine mesh created in GAMBIT.	25
Figure 3.3.	Plot of residuals for k-epsilon solver method as the iterations proceeds.	27
Figure 4.1.	Counters of mass fraction of Oxygen (O_2) in Water for water velocity of 0.1 m/s and air velocity of 0.1 m/s.	28
Figure 4.2.	Contours of volume fraction of liquid for water velocity of 0.1 m/s and air velocity of 0.1 m/s.	29
Figure 4.3.	Gas holdup vs. water velocity for constant air velocity of 0.1m/s.	30
Figure 4.4.	Gas holdup vs. air velocity for constant liquid velocity of 0.1m/s.	30
Figure 4.5.	Liquid holdup vs. water velocity for constant air velocity of 0.1m/s.	30
Figure 4.6.	Liquid holdup vs. water velocity for constant liquid velocity of 0.1m/s.	30
Figure 4.7.	Velocity vectors by velocity magnitude in liquid and the magnified view of the boxed part.	31
Figure 4.8.	Velocity vectors by velocity magnitude in air and the magnified view of the boxed part.	31
Figure 4.9.	XY plot of velocity profile of water across the cross section of column at height 0.5m.	32
Figure 4.10.	XY plot of velocity profile of liquid across the cross	

	section of column at height 1m.	32
Figure 4.11.	XY plot of velocity profile of liquid across the cross section of column at height 1.5m.	33
Figure 4.12.	Snapshots of radial velocity of air in the column at different time intervals.	33
Figure 4.13.	Snapshots of axial velocity of air in the column at different time intervals.	34
Figure 4.14.	Contours of static gauge pressure (mixture phase)	34
Figure 4.15.	XY graph of static pressure vs. column height.	34
Figure 4.16.	Mass fraction profile of O2 in air in the column	35
Figure 4.17.	XY Plot of Liquid O2 mass fraction vs. column height.	35
Figure 4.18.	Plot of variation in oxygen transferred to de-aerated water at constant air velocity of 0.1 m/s and various liquid velocities.	36
Figure 4.19.	Plot of variation in oxygen transferred to de-aerated water at constant liquid velocity of 0.1 m/s and various gas velocities.	36
Figure 4.20.	Comparison graph between experimental and simulated results.	37

LIST OF TABLES

TABLE NO.	DESCRIPTION	PAGE NO.
Table 1.1.	Few applications of gas-liquid bubble column.	4
Table 1.2.	Recent applications of CFD in modeling hydrodynamics and mass transfer.	10
Table 3.1a.	Properties of air, water used in experiment.	23
Table 3.1b.	Species Mass Fraction in the two phases.	23
Table 3.2	Model constants used for simulation.	25

NOMENCLATURE

a_s	the specific gas–liquid interfacial area, m^2
C_l	the bulk liquid phase oxygen concentration, mole l^{-1}
$C_{l\text{-}int}$	the liquid phase oxygen concentration at the interface, mole l^{-1}
$C_{g\text{-}int}$	the vapor phase oxygen concentration at the interface, mole l^{-1}
C_g	the bulk vapor phase oxygen concentration, mole l^{-1}
d_s	sauter mean bubble diameter, m
F	body force, N
g	Acceleration due to gravity, m sec^{-2}
G_k	the generation of turbulence kinetic energy due to the mean velocity gradients
G_b	the generation of turbulence kinetic energy due to buoyancy
H	the Henry's law constant
J	the oxygen flux, kg s^{-1}
k_g	the vapor phase mass transfer coefficient, $m^3\ m^{-2}s^{-1}$
k_l	the liquid phase mass transfer coefficient, $m^3\ m^{-2}s^{-1}$
K_l	the overall mass transfer coefficient based on liquid phase driving force, $m^3\ m^{-2}s^{-1}$
K_g	the overall mass transfer coefficient based on gas phase driving force, $m^3\ m^{-2}s^{-1}$
k_{eff}	effective conductivity, W $m^{-1}\ K^{-1}$
k_t	turbulent thermal conductivity, W $m^{-1}\ K^{-1}$
k	turbulence kinetic energy, J
R_i	the net rate of production of species i by chemical reaction
S_i	the rate of creation by addition from the dispersed phase plus any user-defined sources
Y_M	represents the contribution of the fluctuating dilatation in compressible turbulence to the overall dissipation rate
y	Distance, m

Greek Symbols

$\vec{v}_m$	mass-averaged velocity, m s^{-1}
ρ_m	mixture density, kg m^{-3}
ρ_k	Density of phase k= g (gas), l (liquid), kg m^{-3}
α_k	volume fraction of phase k
n	number of phases
μ_m	viscosity of the mixture, Pa s
ε_g	gas holdup in fluidized bed, -
ε_l	liquid holdup in fluidized bed, -
ε_k	Volume fraction of phase k= g (gas), l (liquid)
μ_L	liquid viscosity, Pa s
$\upsilon_{dr,k}$	drift velocity for secondary phase k, m s^{-1}
ε	rate of dissipation of turbulent kinetic energy, m^2s^{-3}
σ_k	and are the turbulent Prandtl numbers for k and ε
σ_ε	the turbulent Prandtl number for ε

Abbrevation

CFD	computational fluid dynamics

CHAPTER 1
INTRODUCTION AND LITERATURE REVIEW

1.1 Introduction

Bubble columns are intensively used as multiphase contactors and reactors in chemical, biochemical and petrochemical industries. They provide several advantages during operation and maintenance such as high heat and mass transfer rates, compactness and low operating and maintenance costs. Bubble column reactors belong to the general class of multiphase reactors which consist of three main categories namely, the trickle bed reactor (fixed or packed bed), fluidized bed reactor, and the bubble column reactor. A bubble column reactor is basically a cylindrical vessel with a gas distributor at the bottom. The gas is sparged in the form of bubbles into either a liquid phase or a liquid–solid suspension. These reactors are generally referred to as slurry bubble column reactors when a solid phase exists. Bubble columns are used especially in chemical processes involving reactions such as oxidation, chlorination, alkylation, polymerization and hydrogenation, in the manufacture of synthetic fuels by gas conversion processes and in biochemical processes such as fermentation and biological wastewater treatment (Kantarci et al., 2005).

Much works have been devoted to either kinetic modeling or fluid dynamics in chemical and biochemical process engineering. Most works have been performed under the assumption of idealized conditions. Either the reactor was assumed to be an ideal model case or the fluid dynamics was considered in a realistic way, but mass transfer and chemical reaction were omitted. Despite the widespread application of bubble columns and substantial research efforts devoted to understand their behavior, detailed knowledge on the fluid flow, mass transfer and chemical reactions as well as their interactions are still lacking. However, the scale-up of bubble column is still poorly understood because of the complexity of the flow patterns and their unknown behavior under different sets of design parameters. Gas-liquid flow in bubble column reactors is characterized by a combination of inherently unsteady complex processes with widely varying spatial and temporal scales. Understanding the complexity of the fluid dynamics in bubble column and airlift reactors is important due to their application in the chemical and bioprocess industries (Mousavi et al., 2007).

Knowledge of the hydrodynamics of such reactors helps to determine the efficiency of biochemical production rates through transport processes such as inter-phase oxygen transfer, mixing of nutrients and reactants plus the effects that pH has on micro-organisms growth, metabolic pathways and cell lyses. Also of importance is knowledge of the influence of the biomass on the gas phase through inter-phase interactions and the impact the biomass has on the liquid phase viscosity (Blažej et al., 2004).

Study of the flow hydrodynamics in bubble columns involves the use of experimental techniques and computational fluid dynamics (CFD). The potential of CFD for describing the hydrodynamics of bubble columns has been established by several publications, for example (Mousavi et al., 2007). An important advantage of the CFD approach is that column geometry and scale effects are automatically accounted. The success of the CFD simulation strategy is however crucially dependent on the proper modeling of the momentum exchange, or drag coefficient between the gas and liquid phases. CFD modeling of gas-liquid two-phase flows has shown remarkable progress over the last decade. The methods developed include the volume of fluid methods, dispersed phase models, Eulerian two-fluid models, and the algebraic slip mixture models. The two most common approaches to modeling bubble columns are the Euler-Euler or two-fluid approach and the Euler-Lagrange or discrete bubble approach. In the Euler-Euler approach, both phases (the continuous liquid phase and the dispersed gas phase) are modeled as two inter-penetrating continua. In the Euler-Lagrange approach on the other hand, the volume averaged Navier-Stokes equations are used to describe the motion of the liquid phase and each bubble is tracked on basis of a balance of forces acting upon (Mousavi et al., 2007).

1.2 Bubble Column reactors

Bubble columns, in which gas bubbles rise through a liquid, are known as excellent reactors for processes which require large interfacial area for gas–liquid mass transfer and efficient mixing for reacting species. Oxidation, hydrogenation, chlorination and alkylation are examples of liquid bulk processes being performed in bubble-column reactors. The distinct advantage of bubble column over other gas-liquid contactors are its simple design and construction, low operation costs, excellent heat and mass transfer characteristics and high mixing ability (Ekambara et al., 2005).

The hydrodynamics in bubble columns is determined by the bubble rise and hence bubble size distribution and gas hold-up. Three regimes generally occur in bubble columns. A schematic representation of these three flow regimes is shown in Fig. 1.1. The homogeneous regime is obtained at low gas superficial velocities. Its bubble size distribution is monomodal, narrow and is only influenced by the type of gas sparger used, and coalescence and break-up phenomena are negligible. In aqueous systems, the rise velocity of the spherical and ellipsoidal bubbles is about 0.18-0.3 m. Liquid up flow is found in the wake of bubbles and liquid flows down in between the bubbles and near the walls. When the superficial gas velocity is increased, the heterogeneous regime is obtained, in which coalescence and break-up occur more frequently. Bubbles with different shapes and sizes are observed in the column. Large bubbles travel in the center of the column whereas smaller bubbles move along the walls or are tracked in the wakes of large bubbles. The undesirable slug flow regime is observed at even higher superficial gas velocity and/or in particular, when the column diameter is smaller than 0.15 m. In this regime, very large bubbles, i.e., slugs span the entire cross section of the bubble column. The slug flow regime is frequently encountered in pipelines used to transport gas-oil mixtures (Zhang, 2007).

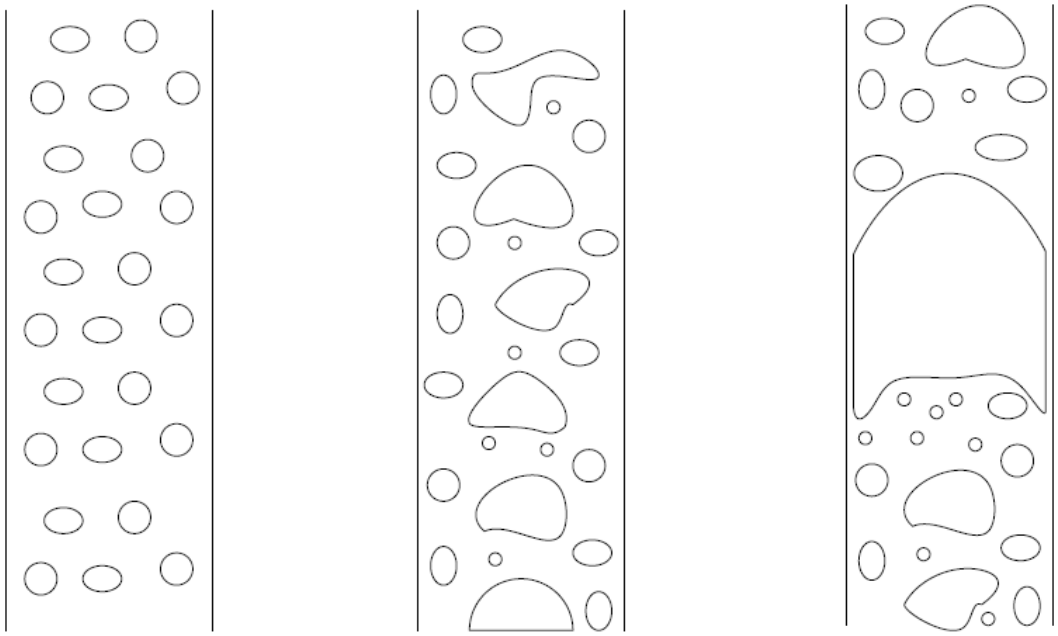

Fig. 1.1. The flow regime observed in gas-liquid bubble column reactors: bubbly flow or homogeneous regime (left); heterogeneous regime (middle) and slug flow regime (right) (Zhang, 2007).

1.3 Applications of gas-liquid bubble column

They are used especially in chemical processes involving reactions such as oxidation, chlorination, alkylation, polymerization and hydrogenation, in the manufacture of synthetic fuels by gas conversion processes and in biochemical processes such as fermentation and biological wastewater treatment. Some very well-known chemical applications are the famous Fischer–Tropsch process which is the indirect coal liquefaction process to produce transportation fuels, methanol synthesis, and manufacture of other synthetic fuels which are environmentally much more advantageous over petroleum- derived fuels. An important application area of bubble columns is their use as bioreactors in which microorganisms are utilized in order to produce industrially valuable products such as enzymes, proteins, antibiotics, etc (Kantarci et al., 2005). Other important applications include halogenation, hydrohalogenation, ammonolysis, ozonolysis, carbonylation, hydroformylation, carboxylation, hydrometallurgical operations, steel ladle stirring, column flotation etc (Joshi, 2001). Some of the typical applications are listed below.

Table 1.1. Few applications of gas-liquid bubble column.

Applications	Process type	References
Catalytic chlorination	chemical	Lohse et al. (1983)
Production of thienamycin	biochemical	Arcuri et al. (1986)
Manufacture of Acetic acid using Acetobacter aceti	biochemical	Sun and Furusaki (1990)
Production of root cultures of Hyoscyamus muticus	biochemical	Bordonaro and Curtis (2000)
Biological wastewater treatment	biochemical	Prakash et al. (2001)
Fischer–Tropsch process to produce transportation fuels, methanol synthesis, and manufacture of other synthetic fuels	chemical	Degaleesan et al. (2001)
Ethanol fermentation using Saccharomyces cerevisiae	biochemical	Ogbonna et al. (2001)
Ferrous biological oxidation	biochemical	Mousavi et al. (2008)

1.4 Mass transfer across gas-liquid interface

The overall mass transfer rate per unit volume of the dispersion in a bubble column is governed by the liquid-side mass transfer coefficient, $k_l a$ assuming that the gas side resistance is negligible. In a bubble column reactor the variation in $k_l a$ is primarily due to variations in the interfacial area. Assuming spherical bubbles, the specific gas–liquid interfacial area is related to the gas holdup, ε_g and the sauter mean bubble diameter, d_s by

$$a_s = \frac{6\epsilon_g}{d_s} \tag{1.1}$$

Thus, a precise knowledge of the gas holdup and bubble size distribution is needed to determine the specific gas– liquid interfacial area. In gas–liquid reactors, mass transfer from the gas to liquid phase is the most important goal of the process. The volumetric mass transfer coefficient is a key parameter in the characterization and design of both industrial stirred and non-stirred gas–liquid reactors. However, very few data are found dealing separately with mass transfer coefficient (k_l) and interfacial area in bubble columns or stirred reactors. Most investigations performed are limited to the determination of the volumetric mass transfer coefficient, $k_l a$, which is the product of the liquid mass transfer coefficient 'k_l' and interfacial area 'a'. Unfortunately, this parameter is global and not sufficient to provide an understanding of the mass transfer mechanisms. The separation of the parameters 'k_l' and 'a' should be considered for better comprehension of the gas–liquid mass transfer mechanisms. It also allows us to identify which parameter (k_l or a) controls the mass transfer (Kantarci et al., 2005).

Fig. 1.2 describes mass transfer between a liquid with no insoluble solids and a gas. In the figure, C_l is the bulk liquid phase oxygen concentration, $C_{l\text{-}int}$ is the liquid phase oxygen concentration at the interface, $C_{g\text{-}int}$ is the vapor phase oxygen concentration at the interface, and C_g is the bulk vapor phase oxygen concentration.

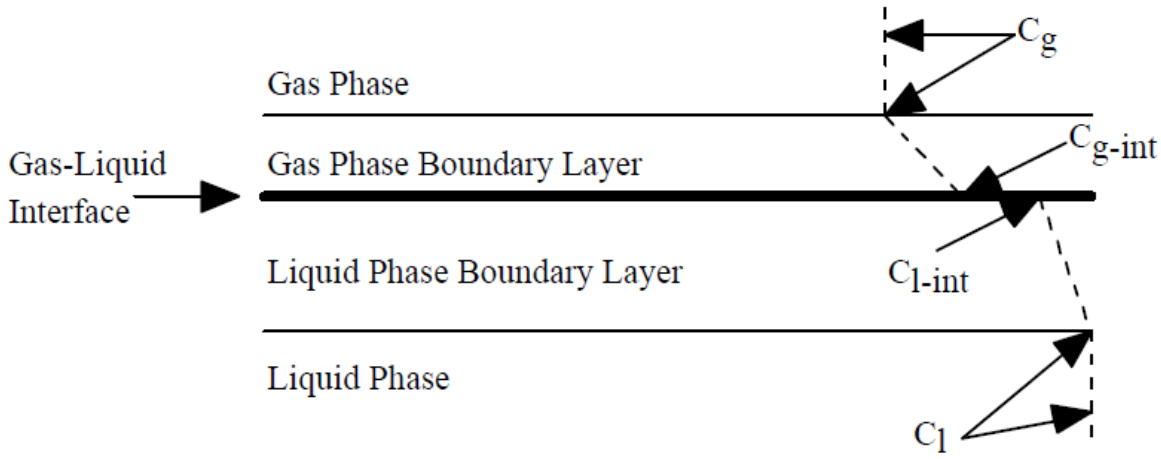

Fig. 1.2. Interphase gas liquid mass transfer.

Diffusion Controlled Mass Transfer

A boundary layer is a region close to the interface where both phases influence the mass transfer process. Oxygen is transported from the bulk vapor phase to the vapor boundary layer. (The edge of the boundary layer is generally defined as the point at which the concentration is within 1% of the bulk phase concentration.) Within the liquid phase boundary layer, mass transfer occurs from the edge of the boundary layer to the vapor-liquid interface by diffusion and the flux is described by Eq. (1.2).

$$J = \frac{a\ A\ \Delta C}{\Delta y} \tag{1.2}$$

where J is the oxygen flux, a is the molecular diffusivity, A is the surface area, C is the oxygen concentration, and y is distance.

At the vapor-liquid interface, the vapor and liquid are in equilibrium. The oxygen is also transported from the vapor-liquid interface to the edge of the liquid boundary layer by diffusion, and then transported from the liquid boundary layer to the bulk liquid.

The flux across either the liquid or vapor phase boundary layer can be changed by changing the molecular diffusivity, the surface area, the concentration difference across the boundary layer (ΔC), or the boundary layer thickness.

The term a/Δy can be replaced by a constant, k, which is called the mass transfer coefficient. The mass transfer coefficient can be changed by changing the boundary layer thickness or the molecular diffusivity. As the oxygen is transported from the vapor phase to the liquid phase, the

vapor phase boundary layer is replenished from the bulk vapor. If the bulk vapor does not replenish the oxygen lost from the vapor phase boundary layer, the vapor phase boundary layer thickness will increase and the mass transfer coefficient will decrease. If the bulk vapor transports oxygen to the vapor boundary layer faster than it is removed, the vapor boundary layer thickness decreases and the mass transfer coefficient increases.

Convective Mass Transfer

Convective mass transfer from the gas phase to the liquid phase and vice versa can be described with a mass transfer coefficient. The flux is equal to the product of the mass transfer coefficient, the surface area, and the concentration difference (Flux = k A ΔC). The concentration difference can be the concentration difference across the gas phase boundary layer, the concentration difference across the liquid phase boundary layer, the concentration difference between the bulk vapor and the vapor which would be in equilibrium with the bulk liquid, or the concentration difference between the bulk liquid and the liquid which would be in equilibrium with the bulk vapor. If the concentration difference across the gas phase boundary layer is used, the mass transfer coefficient is called a gas phase mass transfer coefficient. If the concentration difference across the liquid phase boundary layer is used, the mass transfer coefficient is called a liquid phase mass transfer coefficient. If the concentration difference between the bulk vapor and the vapor which would be in equilibrium with the bulk liquid is used, the mass transfer coefficient is called an overall mass transfer coefficient. If the concentration difference between the bulk liquid and the liquid which would be in equilibrium with the bulk vapor is used, the mass transfer coefficient is also called an overall mass transfer coefficient.

The vapor phase mass transfer coefficient is described by Eq. (1.3), and the liquid phase mass transfer coefficient is described by Eq. (1.4).

$$J = k_g(C_{g-int} - C_g) \tag{1.3}$$

$$J = k_l(C_l - C_{l-int}) \tag{1.4}$$

In Eqs. (1.3) and (1.4), J is the flux, A is the interfacial area, kg is the vapor phase mass transfer coefficient, and kl is the liquid phase mass transfer coefficient.

Since $C_{g\text{-}int}$ and $C_{l\text{-}int}$ are difficult to determine, while C_g and C_l can usually be measured or calculated, the overall mass transfer coefficient can be described by Eqs. (1.5) and (1.6).

$$J = K_g A\left(C_g^* - C_g\right) = K_g A(H\, C_l - C_g) \tag{1.5}$$

$$J = K_l A(C_l - C_l^*) = K_l A(C_l - {}^{C_g}/_{H}) \tag{1.6}$$

In Eqs. (1.5) and (1.6), K_g is the overall mass transfer coefficient based on vapor phase driving force, K_l is the overall mass transfer coefficient based on liquid phase driving force, C_g* is the concentration of oxygen in the vapor phase which is in equilibrium with the bulk liquid, C_l* is the liquid phase oxygen concentration which is in equilibrium with the bulk vapor, and H is the Henry's law constant. Since at steady state, the fluxes calculated with Eqs. (1.3) – (1.6) are equal, relationships between the mass transfer coefficients described in the equations are derived in the literature and shown in Eqs. (1.7) – (1.9).

$${}^{1}/_{K_g} = {}^{1}/_{k_g} + {}^{H}/_{k_l} \tag{1.7}$$

$${}^{1}/_{K_l} = {}^{1}/_{k_l} + {}^{1}/_{H k_g} \tag{1.8}$$

$$K_l = H\, K_g \tag{1.9}$$

The overall mass transfer coefficient is a function of the liquid phase and vapor phase mass transfer coefficients; that is, the combined resistance to mass transfers across both the liquid and vapor boundary layers. If the vapor phase mass transfer coefficient (k_g) is much larger than the liquid phase mass transfer coefficient (k_l), the overall mass transfer coefficient (K_l) is approximately equal to the liquid phase mass transfer coefficient: in other words, because the resistance to mass transfer in the vapor phase is low, the liquid phase resistance controls the mass transfer process. Therefore, in a system containing oxygen at low concentration, the oxygen will be transferred from the vapor phase boundary layer to the liquid phase faster than it can be transferred from the bulk vapor to the vapor phase boundary layer. The vapor phase boundary layer will become depleted in oxygen, and increase in thickness. The thicker boundary layer will lead to a smaller mass transfer coefficient and a lower mass transfer rate.

Eqs. (1.10) and (1.11) describe the relationship between overall mass transfer coefficients and individual phase mass transfer coefficients in this work.

$$K_g \cong {}^{k_l}/_{H} \tag{1.10}$$

$$K_l \cong k_l \tag{1.11}$$

The reciprocal of the product of the mass transfer coefficient and area is often referred to as the resistance to mass transfer. The overall resistance to mass transfer through both the liquid and vapor boundary layers is reflected in the overall mass transfer coefficient, either K_g or K_l.

1.5 Mass transfer phenomenon studied in gas-liquid bubble column

There are many industrial processes that involve gas-liquid dispersion in stirred tanks, *e.g.* in fine-chemical manufacturing, or in biochemical fermentations. For economic and safety reasons, reliable models are needed for the scale-up and design of such reactors.

Yet successful design and scale-up of bubble column reactors remain difficult due to the complex interaction and mixing of phases. As one of the key determinants of reactor performance, the gas–liquid mass transfer in bubble columns is directly affected by the hydrodynamics, phase mixing, and physical properties. In the ongoing effort to reduce uncertainty, there has been a large body of mass transfer research covering various conditions. One of the most important problems in modeling gas-liquid dispersions is the prediction of bubble size and gas-liquid interfacial area (Gimbun et al., 2009). The distribution of bubble sizes varies inside the stirred tank depending on the spatial position. Besides, only a limited number of mass transfer studies separately measured the liquid side mass transfer coefficient, k_1, and the interfacial area, a, although these two parameters help understand the underlying phenomena. More importantly, the reported effects of operating pressure and superficial gas velocity on k_1 are not consistent, the k_1 values were found to decrease with the operating pressure, while some found the k_1 values to be independent of the pressure. Regarding the dependence of k_1 on the superficial gas velocity, u_g, the conclusions vary from the k_1 values being independent of u_g, For mass transfer coefficient measurements in bubble columns, the driving force of gas–liquid mass transfer is usually produced by dynamic change in the gas or liquid input (pulse or step), by pressurizing the gas phase, or by the presence of chemical reactions. Of late, computational fluid dynamics (CFD) has been promoted as a useful tool for better understanding of the multiphase reactors for precise design and scale up. The report on the computational models for the mass transfer in bubble columns is limited. Thus, there exist many grey areas requiring further extensive fundamental studies for the gas-liquid contacting systems (Han and Al-Dahhan, 2007).

1.6 Recent applications of CFD in modeling hydrodynamics and mass transfer

Although mass transfer and hydrodynamics in bubble columns are important phenomenon, very little computational work has been done on it till now. Following is the work done by various researchers using CFD in a variety of systems using varied computational packages.

Table 1.2. Recent applications of CFD in modeling hydrodynamics and mass transfer

Authors	**Multiphase Approach**	**Models Used**	**Parameter Studied**
Sokolichin et al. (1997)	2D Euler–Euler Euler–Lagrangian	Laminar model	Flow pattern
Pfleger et al. (1999)	2D, 3D Euler–Euler	Std. k–ε model	Hydrodynamics
Cockx et al. (2000)	Eulerian-Eulerian	ASTRID used	Predict accurately dissolved gas concentration in reactors
Deen et al. (2001)	3D Euler–Euler	Std. k–ε model and LES	Hydrodynamics
Ekambara et al. (2005)	1D, 2D, 3D approach	k-eps turbulence model	Three models studied for axial liquid velocity and the fractional gas hold-up profiles
Lopes and Quinta-Ferreira (2007)	3D approach Euler-Euler model	Eulerian k-fluid model	Investigated complex behavior involving hydrodynamics and ferrous biological oxidation in a gas–liquid bubble column reactor
Kerdouss et al.(2008)	2D Eulerian–Eulerian approach	Population balance model, dispersed k–e turbulent model, Multiple Reference Frame (MRF) Model	Effect of bubble breakup and coalescence in the tank
Fayollea et al. (2007)	2D Euler–Euler model	Eulerian two-fluid model derived from Reynolds average Navier–Stokes equations, The k–ε	Optimized aeration in the activated sludge processes to predict flow and oxygen transfer characteristics

		dispersed model for turbulence, Tchen-theory correlations are respectively applied to the continuous and dispersed phase	in aeration tanks equipped with fine bubble diffusers and axial slow speed mixers
Tabib et al. (2008)	Eulerian–Eulerian approach	Three different turbulence closure (k–ε, RSM and LES) models	Sensitivity of different interphase forces (drag, lift, turbulent dispersion and added mass) is accessed. highlights the importance of choosing the C_L value and the drag law in accordance with the bubble size
Gimbun et al. (2009)	Eulerian-Eulerian two-fluid model	Population Balance Method, the drag coefficient of spherical and distorted bubbles was modeled using the Ishii-Zuber equations	Gas liquid hydrodynamics and local bubble sizes, gas dispersion and mass transfer coefficient comparison between the CD-6 impeller and the Rushton turbine
Mousavi et al. (2009)	Volume of fluid (VOF) method was used to predict the fluid volume fraction in a 3D geometry.	Surface tension model, the continuum surface force model	The concentration profiles and liquid velocity field, effect of inlet air velocity on the fluid velocity field
Moilanen (2009)	The complex models were implemented through FORTRAN 77 routines.	The multicomponent mass transfer model was linked to an in-house program called Flowbat	Physical properties, vapour-liquid equilibrium, gas holdup, gas-liquid mass transfer, bubble size distributions, local mixing times, flow fields and bubble swarm interactions.
Duran et al. (2009)	_	Different	Different models were

		hydrodynamic models including laminar, standard k–e, realizable k–e, Reynolds stress (RSM), and the Abe-Kondoh-Nagano (AKN) (a low Reynolds number turbulence model) were used	evaluated against experimental data in terms of their mass transfer predication capabilities
Haroun et al. (2010)	Volume of fluid method	The numerical code used for determining the solubility of the chemical species at the interface is the JADIM code. The interfacial force is solved using the classical continuum surface force model.	Study of reactive laminar liquid film

The current design procedure of bubble columns is closer to empiricism rather than the much-desired procedures based on fundamental understanding of the hydrodynamic parameters and its relationship with the process performance. In order to reduce the empiricism, the last decade has seen a vigorous effort in understanding the fluid mechanics in bubble columns to know the relationship between the flow pattern and the design objective. In one way, this can be achieved by using computational fluid dynamics for understanding the flow pattern and extending it for calculating the hydrodynamic parameters.

In view of the fact that the mass transfer in gas-liquid systems is an essential sub-process in many industrial processes, the developing of an understanding to obtain optimum conditions for this process is critical. Till now, very little computational work has been found to be done in this field. In this thesis an attempt has been made to understand the gas-liquid bubble column hydrodynamics and mass transfer.

CHAPTER 2
CFD IN MULTIPHASE MODELING

2.1 CFD (Computational Fluid Dynamics)

CFD is one of the branches of fluid mechanics that uses numerical methods and algorithms to solve and analyze problems that involve fluid flows. Computers are used to perform the millions of calculations required to simulate the interaction of fluids and gases with the complex surfaces used in engineering. However, even with simplified equations and high speed supercomputers, only approximate solutions can be achieved in many cases. More accurate codes that can accurately and quickly simulate even complex scenarios such as supersonic or turbulent flows are an ongoing area of research (Mahapatra and Rakh, 2007).

The result of CFD analysis is relevant engineering data which are used in conceptual studies of new designs, detail product development, troubleshooting and design. The various general purpose CFD packages in use are FLUENT, CFX, STAR-CD, PHONIX, FLOW3D etc. Most of these packages are based on finite volume method and are used to solve fluid flow and mass transfer problems (Pandey, 2010).

2.2 Advantages of CFD

Major advancements in the area of gas-solid multiphase flow modeling offer substantial process improvements that have the potential to significantly improve process plant operations. Prediction of gas solid flow fields, in processes such as pneumatic transport lines, risers, fluidized bed reactors, hoppers and precipitators are crucial to the operation of most process plants. Up to now, the inability to accurately model these interactions has limited the role that simulation could play in improving operations. In recent years, computational fluid dynamics (CFD) software developers have focused on this area to develop new modeling methods that can simulate gas-liquid-solid flows to a much higher level of reliability. As a result, process industry engineers are beginning to utilize these methods to make major improvements by evaluating alternatives that would be, if not impossible, too expensive or time-consuming to trial on the plant floor. Over the past few decades, CFD has been used to improve process design by allowing engineers to simulate the performance of alternative configurations, eliminating guesswork that would normally be used to establish equipment geometry and process conditions. The use of CFD enables engineers to obtain solutions for problems with complex geometry and

boundary conditions. A CFD analysis yields values for pressure, fluid velocity, temperature, and species or phase concentration on a computational grid throughout the solution domain (Kumar, 2009).

Advantages of CFD can be summarized as:

1. It provides the flexibility to change design parameters without the expense of hardware changes. It therefore costs less than laboratory or field experiments, allowing engineers to try more alternative designs than would be feasible otherwise.
2. It has a faster turnaround time than experiments.
3. It guides the engineer to the root of problems, and is therefore well suited for trouble-shooting.
4. It provides comprehensive information about a flow field, especially in regions where measurements are either difficult or impossible to obtain.

2.3 CFD modeling of multiphase systems

This section focuses on CFD modeling of multiphase systems. Following are some examples of multiphase systems:

- Bubbly flow examples: absorbers, aeration, airlift pumps, cavitations, evaporators, flotation and scrubbers.
- Droplet flow examples: absorbers, atomizers, combustors, cryogenic pumping, dryers, evaporation, gas cooling and scrubbers.
- Slug flow examples: large bubble motion in pipes or tanks.

2.4 Approaches for numerical calculations of multiphase flows

In the case of multiphase flows currently there are two approaches for the numerical calculations:

1. Euler-Lagrange approach
2. Euler-Euler approach

2.4.1 The Euler-Lagrange Approach

The Lagrangian discrete phase model follows the Euler-Lagrange approach. The fluid phase is treated as a continuum by solving the time-averaged Navier- Stokes equations, while the dispersed phase is solved by tracking a large number of particles, bubbles, or droplets through the calculated flow field. The dispersed phase can exchange momentum, mass and energy with the fluid phase. A fundamental assumption made in this model is that the dispersed second phase

occupies a low volume fraction, even though high mass loading, mass of particle >= mass of fluid is acceptable. The particle or droplet trajectories are computed individually at specified intervals during the fluid phase calculation. This makes the model appropriate for the modeling of spray dryers, coal and liquid fuel combustion, and some particle laden flows, but inappropriate for the modeling of liquid-liquid mixtures, fluidized beds or any application where the volume fraction of the second phase is not negligible (Mahapatra and Rakh, 2007).

2.4.2 The Euler-Euler Approach

In the Euler-Euler approach the different phases are treated mathematically as interpenetrating continua. Since the volume of a phase cannot be carried occupied by the other phases, the concept of the volume fraction is introduced. These volume fractions are assumed to be continuous functions of space and time and their sum is equal to one. Conservation equations for each phase are derived to obtain a set of equations, which have similar structure for all phases. These equations are closed by providing constitutive relations that are obtained from empirical information or in the case of granular flows by application of kinetic theory (Kumar, 2009).

There are three different Euler-Euler multiphase models available: The volume of fluid (VOF) model, the Mixture model and the Eulerian model.

2.4.2.1 The VOF Model

The VOF model is a surface tracking technique applied to a fixed Eulerian mesh. It is designed for two or more immiscible fluids where the position of the interface between the fluids is of interest. In the VOF model, a single set of momentum equations is shared by the fluids and the volume fraction of each of the fluids in each computational cell is tracked throughout the domain. The applications of VOF model include stratified flows, free surface flows, filling, sloshing, and the motion of large bubbles in a liquid, the motion of liquid after a dam break, the prediction of jet breakup (surface tension) and the steady or transient tracking of any liquid- gas interface (Kumar, 2009).

2.4.2.2 The Mixture Model

The mixture model is designed for two of more phases (fluid or particulate). As in the Eulerian model, the phases are treated as interpenetrating continua. The mixture model solves for the mixture momentum equation and prescribes relative velocities to describe the dispersed phase.

Applications of the mixture model include particle-laden flows with low loading, bubbly flows, and sedimentation and cyclone separators. The mixture model can also be used without relative velocities for the dispersed phase to model homogenous multiphase flow (Kumar, 2009).

2.4.2.3 The Eulerian Model

The Eulerian model is the most complex of the multiphase models. It solves a set of n momentum and continuity equations for each phase. Couplings are achieved through the pressure and inter phase exchange coefficients. The manner in which this coupling is handled depends upon the type of phases involved; granular (fluid-solid) flows are handled differently than non-granular (fluid-fluid) flows. For granular flows, the properties are obtained from application of kinetic theory. Momentum exchange between the phases is also dependent upon the type of mixture being modeled. Applications of the Eulerian Multiphase Model include bubble columns, risers, particle suspension, and fluidized beds (Kumar, 2009).

2.5 Choosing a multiphase model

The first step in solving any multiphase problem is to determine which of the regimes best represent the flow. General guidelines provides some broad guidelines for determining the/appropriate models for each regime, and detailed guidelines provides details about how to determine the degree of interphase coupling for flows involving bubbles, droplets or particles, and the appropriate models for different amounts of coupling. In general, once that the flow regime is determined, the best representation for a multiphase system can be selected using appropriate model based on following guidelines (Fluent doc., 2006).

Additional details and guidelines for selecting the appropriate model for flows involving bubbles particles or droplets can be found.

- For bubble, droplet and particle-laden flows in which dispersed-phase volume fractions are less than or equal to 10% use the discrete phase model.
- For bubble, droplet and particle-laden flows in which the phases mix and / or dispersed phase volume fractions exceed 10% use either the mixture model.
- For slug flow, use the VOF model.
- For stratified / free-surface flows, use the VOF model.
- For pneumatic transport use the mixture model for homogenous flow or the Eulerian Model for granular flow.

- For fluidized bed, use the Eulerian Model for granular flow.
- For slurry flows and hydro transport, use Eulerian or Mixture model.
- For sedimentation, use Eulerian Model.

Depending on above guidelines following approach was chosen to carry out the simulation of gas-liquid bubble column.

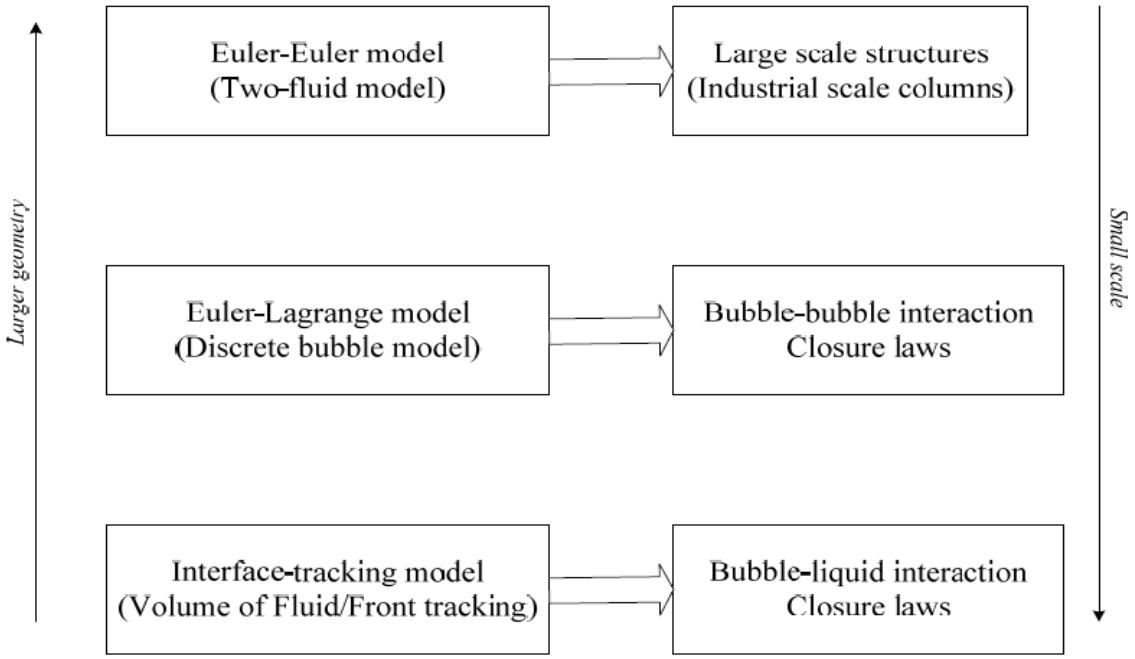

Fig. 2.1. Multi-level modeling concept for fundamental hydrodynamic models of gas-liquid flow in bubble columns (Zhang, 2007).

Detailed information of bubble motion and deformation as well as interfacial closure laws can be obtained by interface tracking models, which solve the instantaneous Navier-Stokes equations to obtain the gas and liquid flow field with a very high spatial resolution with no empirical constitutive equations. The disadvantage of this model is that the number of bubbles that can be simulated simultaneously is limited (<100 bubbles). Different methods were used for this interface tracking technique.

In the Euler-Lagrange approach, also called discrete bubble model (DBM), the continuous liquid phase is described as a continuum in an Eulerian framework. The dispersed gas phase on the other hand is treated in a Lagrangian way. That is, each individual bubble in the system is tracked by solving Newton's second law. The model has a two-way coupling for the exchange of

momentum between the gas and liquid phase, which can be obtained from interface tracking model based closure relations. As each individual bubble is tracked in the computational domain, breakup and coalescence can be easily implemented in this approach, which makes the E-L method well suited for fundamental investigations of the bubbly flow. The main disadvantage of the E-L approach is the limitation of the numbers of bubbles (106) and the required computational effort (Zhang, 2007).

In the Euler–Euler approach, also called two-fluid model, both the gas and liquid phases are regarded as two interpenetrating phases, and each phase has its own set of conservation equations of mass, momentum and energy, coupled with some phase interaction terms. The governing equations are derived from various averaging techniques (time averaging, volume averaging and ensemble averaging). Closure equations for the required interfacial exchange terms can be derived using the interface tracking models. The breakup and coalescence should be accounted for through a proper model rather than relatively simple constitutive equations as in the E-L model. The advantage of this approach is that the computational demands are much lower compared to the Euler–Lagrange approach. Thus the Euler-Euler model is preferred in high gas holdup and churn turbulent flows or in industrial scale bubble columns. As this thesis aims to numerically study gas-liquid flows in bubble column with industrial relevance, the Euler-Euler model will be used in this thesis (Zhang, 2007).

CHAPTER 3
CFD SIMULATION OF HYDRODYNAMICS AND GAS LIQUID MASS TRANSFER

3.1 Computational flow model

In the present work, an Mixture multi-fluid model is adopted where gas and liquid phases are all treated as continua, inter-penetrating and interacting with each other everywhere in the computational domain. The pressure field is assumed to be shared by all the three phases, in proportion to their volume fraction. The motion of each phase is governed by respective mass and momentum conservation equations. The mixture model can model n phases (fluid or particulate) by solving the momentum, continuity, and energy equations for the mixture, the volume fraction equations for the secondary phases, and algebraic expressions for the relative velocities. The mixture model is a good substitute for the full Eulerian multiphase model in several cases. A full multiphase model may not be feasible when there is a wide distribution of the particulate phase or when the interphase laws are unknown or their reliability can be questioned. A simpler model like the mixture model can perform as well as a full multiphase model while solving a smaller number of variables than the full multiphase model.

Continuity equation

$$\frac{\partial}{\partial t}(\rho_m) + \nabla \cdot (\rho_m \vec{v}_m) = 0 \tag{3.1}$$

where υ_m is the mass-averaged velocity

$$\vec{v}_m = \frac{\sum_{k=1}^{n} \alpha_k \rho_k \vec{v}_k}{\rho_m} \tag{3.2}$$

and ρ_m is the mixture density:

$$\rho_m = \sum_{k=1}^{n} \alpha_k \rho_k \tag{3.3}$$

α_k is the volume fraction of phase k.

Momentum equations

The momentum equation for the mixture can be obtained by summing the individual momentum equations for all phases. It can be expressed as

$$\frac{\partial(\rho_m \vec{v}_m)}{\partial t} + \nabla \cdot (\rho_m \vec{v}_m \vec{v}_m) = -\nabla p + \nabla \cdot [\mu_m (\nabla \vec{v}_m + \nabla \vec{v}_m^T)] +$$
$$\rho_m \vec{g} + \vec{F} + \nabla \cdot \left(\sum_{k=1}^{n} \alpha_k \rho_k \vec{v}_{dr,k} \vec{v}_{dr,k} \right) \quad (3.4)$$

where n is the number of phases, F is a body force, and μ_m is the viscosity of the mixture. $\upsilon_{dr,k}$ is the drift velocity for secondary phase k.

Energy Equation

$$\frac{\partial}{\partial t} \sum_{k=1}^{n} (\alpha_k \rho_k E_k) + \nabla \cdot \sum_{k=1}^{n} \left(\alpha_k \vec{v}_k (\rho_k E_k + p) \right) = \nabla \cdot (k_{eff} \nabla T) + S_E \quad (3.5)$$

Where k_{eff} is the effective conductivity ($\sum \alpha_k$ (k_k + k_t)), where k_t is the turbulent thermal conductivity, defined according to the turbulence model being used). The first term on the right-hand side of Equation represents energy transfer due to conduction. S_E includes any other volumetric heat sources.

3.1.1 Turbulence modeling

Additional transport equations for the turbulent kinetic energy k and its dissipation rate ε were considered: the standard k–ε model was chosen for modeling the turbulence. It has the properties such as robustness and reasonable accuracy for a wide range of industrial applications, with recently developed model improvements that provide better performance in the presence of jets and mixing layers. The upgrading concerns the formulation of the turbulent viscosity and the transport equation for ε.

k–ε models assume a high Reynolds number and fully turbulent flow regime so auxiliary methods are required to model the transition from the thin viscous sub-layer flow region along a wall to the fully turbulent, free stream flow region. The choice of the k- ε standard walls function approach determines that the viscosity affecting the near-wall region is not resolved. Instead, analytical expressions are used to bridge the wall boundary and the fully turbulent flow field: the expression implemented in FLUENT is the logarithmic law of the wall for velocity; corresponding relations are available for temperature and wall heat flux. Wall functions avoid the turbulence model adaptation to the presence of the wall, saving computational resources.

The turbulence kinetic energy, k, and its rate of dissipation, ε, are obtained from the following transport equations:

$$\frac{\partial}{\partial t}(\rho k)+\frac{\partial}{\partial x_i}(\rho k u_i)=\frac{\partial}{\partial x_j}\left[\left(\mu+\frac{\mu_t}{\sigma_k}\right)\frac{\partial k}{\partial x_j}\right]+G_k+G_b-\rho\varepsilon-Y_M+S_k \tag{3.6}$$

and

$$\frac{\partial}{\partial t}(\rho \varepsilon)+\frac{\partial}{\partial x_i}(\rho \varepsilon u_i)=\frac{\partial}{\partial x_j}\left[\left(\mu+\frac{\mu_t}{\sigma_\varepsilon}\right)\frac{\partial \varepsilon}{\partial x_j}\right]+C_{1\varepsilon}\frac{\varepsilon}{k}(G_k+C_{3\varepsilon}G_b)-C_{2\varepsilon}\rho\frac{\varepsilon^2}{k}+S_\varepsilon \tag{3.7}$$

Where G_k represents the generation of turbulence kinetic energy due to the mean velocity gradients, G_b is the generation of turbulence kinetic energy due to buoyancy, Y_M represents the contribution of the fluctuating dilatation in compressible turbulence to the overall dissipation rate. $C_{1\varepsilon}$, $C_{2\varepsilon}$ and $C_{3\varepsilon}$ are constants. σ_k and σ_ε are the turbulent Prandtl numbers for k and ε, respectively. S_k and S_ε are user-defined source terms.

The turbulent (or eddy) viscosity, μ_t, is computed by combining k and ε as follows:

$$\mu_t=\rho C_\mu\frac{k^2}{\varepsilon} \tag{3.8}$$

where C_μ is a constant.

3.1.2 Modeling Species Transport

FLUENT can model the mixing and transport of chemical species by solving conservation equations describing convection, diffusion, and reaction sources for each component species. Multiple simultaneous chemical reactions can be modeled, with reactions occurring in the bulk phase (volumetric reactions) and/or on wall or particle surfaces, and in the porous region.

When you choose to solve conservation equations for chemical species, FLUENT predicts the local mass fraction of each species, Yi, through the solution of a convection-diffusion equation for the i^{th} species. This conservation equation takes the following general form:

$$\frac{\partial}{\partial t}(\rho Y_i)+\nabla\cdot(\rho\vec{v}Y_i)=-\nabla\cdot\vec{J_i}+R_i+S_i \tag{3.9}$$

where R_i is the net rate of production of species i by chemical reaction and Si is the rate of creation by addition from the dispersed phase plus any user-defined sources. An equation of this

form will be solved for N-1 species where N is the total number of fluid phase chemical species present in the system. Since the mass fraction of the species must sum to unity, the N^{th} mass fraction is determined as one minus the sum of the N-1 solved mass fractions. To minimize numerical error, the N^{th} species should be selected as that species with the overall largest mass fraction, such as N_2 when the oxidizer is air.

Mass Diffusion in Turbulent Flows

In turbulent flows, FLUENT computes the mass diffusion in the following form:

$$\vec{J_i} = -(\rho D_{i,m} + \frac{\mu_t}{Sc_t})\nabla Y_i \tag{3.10}$$

where Sc_t is the turbulent Schmidt number. The default Sc_t is 0.7. Note that turbulent diffusion generally overwhelms laminar diffusion, and the specification of detailed laminar diffusion properties in turbulent flows is generally not warranted.

Treatment of Species Transport in the Energy Equation

For many multicomponent mixing flows, the transport of enthalpy due to species diffusion $\nabla \cdot [\sum_{i=1}^{n} h_i \vec{J_i}]$ can have a significant effect on the enthalpy field and should not be neglected. In particular, when the Lewis number for any species is far from unity, neglecting this term can lead to significant errors. FLUENT will include this term by default. Upon completion of the calculation, the following quantities can be reported or displayed:

- Mass fraction of species-n
- Mole fraction of species-n
- Concentration of species-n
- Lam Diff Coef of species-n
- Eff Diff Coef of species-n

3.2 Problem description

The problem consists of a gas-liquid bubble column in which air and liquid (water) enters at the bottom of the domain. The water, the primary phase in column is de-aerated containing 0.4 ppm O_2 concentration. As the air and the water being contacted in the column oxygen is transferred secondary phase (air) to primary phase (de-aerated water) and the oxygen concentration in the water increases. In the present work the aim is to access the dynamics of oxygen concentration in

the column along with the hydrodynamic behavior. The bubble column system taken for the study is cylindrical with height 1.88m and ID 0.1m. It has been assumed that air and de-aerated water enters the column are uniformly distributed at the inlet cross section. Table 3.1a shows the properties of air and de-aerated water and Table 3.1b describes the mass fractions of the components in the two phases.

Properties of Materials used

Table 3.1a. Properties of air, water used in experiment

Phases	Density	Viscosity
Liquid (Water)	998.2 Kg/m3	0.001003 kg/m-s
Gas (Air)	1.225 Kg/m3	1.789*10-05 kg/m-s

Table 3.1b. Species Mass Fraction in the two phases.

Phases	Species Mass Fraction	
	O2	H2O
Air	0.23	0.0001
De-aerated Water	0.0000004	0.999985

3.3 Numerical Methodology

The model equations described in section 3.1 have been solved for the problem as discussed in section 3.2 using the commercial CFD software package Fluent 6.3.26. The modeling and simulation in Fluent involves the following steps. The procedure involves the following steps:

(i) generation of suitable grid system;
(ii) conversion of governing equation into algebraic equations;
(iii) selection of discretization schemes;
(iv) formulation of the discretized equation at every grid location;
(v) formulation of pressure equation;
(vi) development of a suitable iteration scheme for obtaining a final solution.

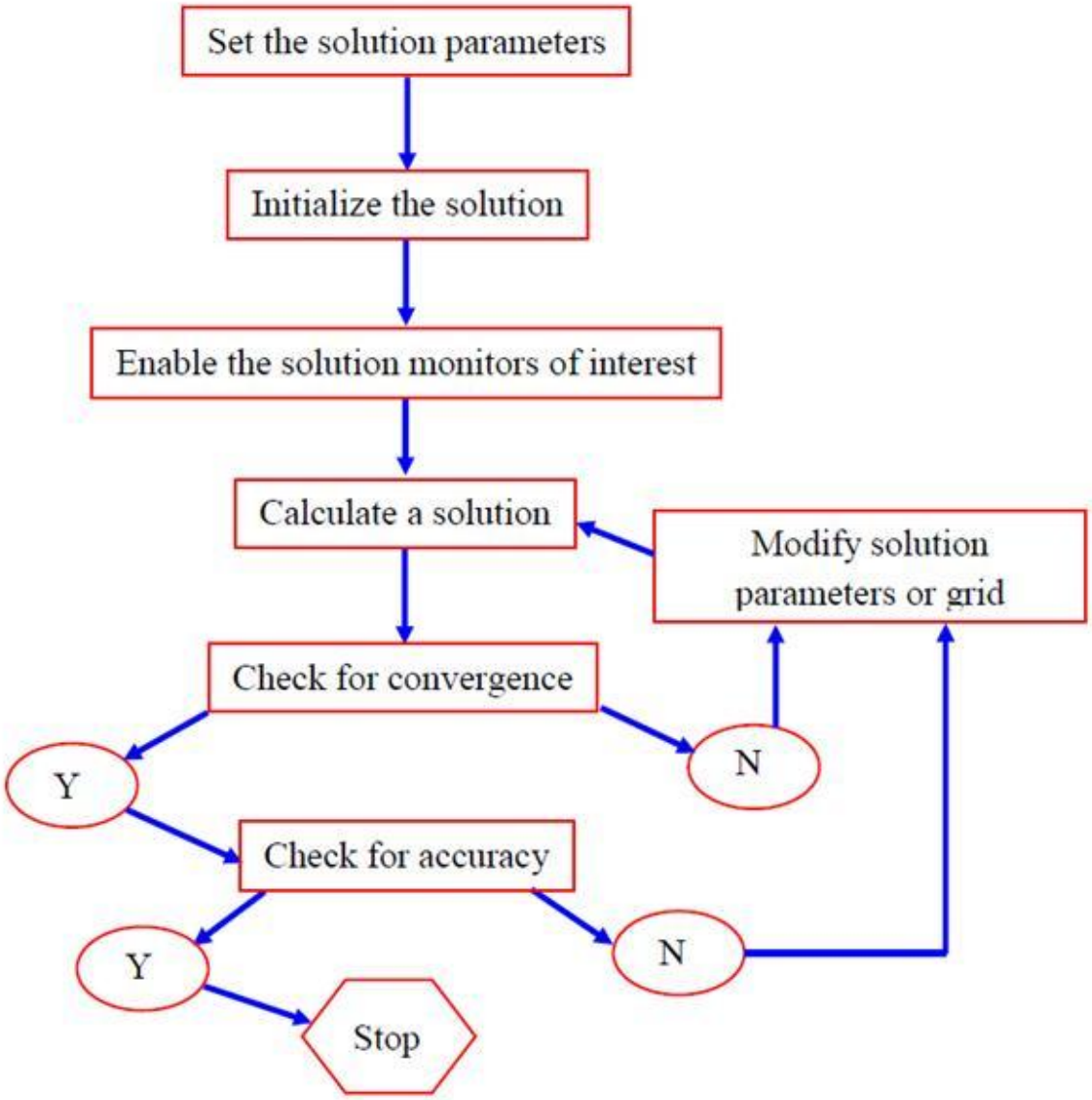

Fig. 3.1. Flowchart showing the general procedure for the simulation using Fluent (Kumar, 2009).

3.3.1 Geometry and Mesh

GAMBIT 2.3.16 was used for making 2D rectangular geometry with width of 0.1m and height 1.88m. Coarse mesh size of 0.01m was taken in order to have 1880 cells (3958 faces) for the whole geometry. Similarly a mesh size of 0.005 m was also used in order to have better accuracy. But using fine mesh results in 7520 cells (15436 faces), which requires even smaller time steps, more number of iterations per time step and 4 times more calculation per iteration for the solution to converge. Also because results obtained in case of coarse grid were in good accordance with experimental outputs, coarse grid was preferred over finer grid for simulation. Use of fine mesh system aims getting more accurate picture of the various simulated parameters. Even then not much change is observed in the results obtained for the two meshes. Fig. 3.2 shows two types of meshing.

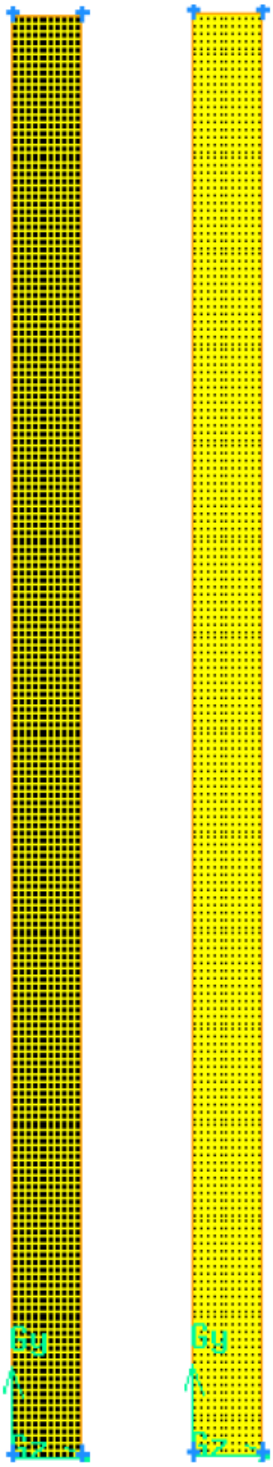

Fig. 3.2. Coarse and fine mesh created in GAMBIT

3.3.2 Selection of models for simulation

FLUENT 6.3.26 was used for simulation. 2D segregated 1st order implicit unsteady solver is used (The segregated solver must be used for multiphase calculations). Standard k-ε mixture multiphase model is used to model turbulence with standard wall functions. Energy Equation is turned on. The model constants are tabulated as:

Table 3.2. Model constants used for simulation

Cmu	0.09
C1-Epsilon	1.44
C2-Epsilon	1.92
TKE Prandtl Number	1
TDR Prandtl Number	1.3
Dispersion Prandtl Number	0.75
Energy Prandtl Number	0.85
Wall Prandtl Number	0.85
Turb Schmidt Number	0.7

- Species Transport Model is enabled to define oxygen as transport species in the water and air. This is done by defining the two materials as Mixture-template in Species Model tab.
- Water is taken as continuous phase while air as secondary phase. Inter-phase interactions Inter-phase interactions formulations used were:

  For Drag Coefficient :

  Air- Liquid: schiller-naumann

  For Slip velocity:

  Air- Liquid: manninen et al.

  Number of Mass transfer mechanisms: 2

  - From Air to Liquid
  - From Liquid to Air
- Velocity Inlet Boundary Conditions:

Air velocity was 0.1m/s and water velocities 0.1m/s with inlet air volume fractions obtained as fraction of air entering in a mixture of gas and liquid as mentioned in Table 3.1b.

- Pressure outlet boundary conditions:

Mixture Gauge Pressure- 0 pascal

Backflow volume fraction for air = 0

3.3.3 Solution

Under relaxation factor for pressure, momentum and volume fraction were taken as 0.3, 0.7, and 0.2 respectively. The discretization scheme for momentum, volume fraction, turbulence kinetic energy and turbulence dissipation rate were all first order upwind. Pressure-velocity coupling scheme was Phase Coupled SIMPLE. The solution was initialized from all zones. Iterations were carried out for time step size of 0.01-0.001 depending on ease of convergence and time required to get the result for interactions in bubble column. During simulation in each time step convergence has been achieved.

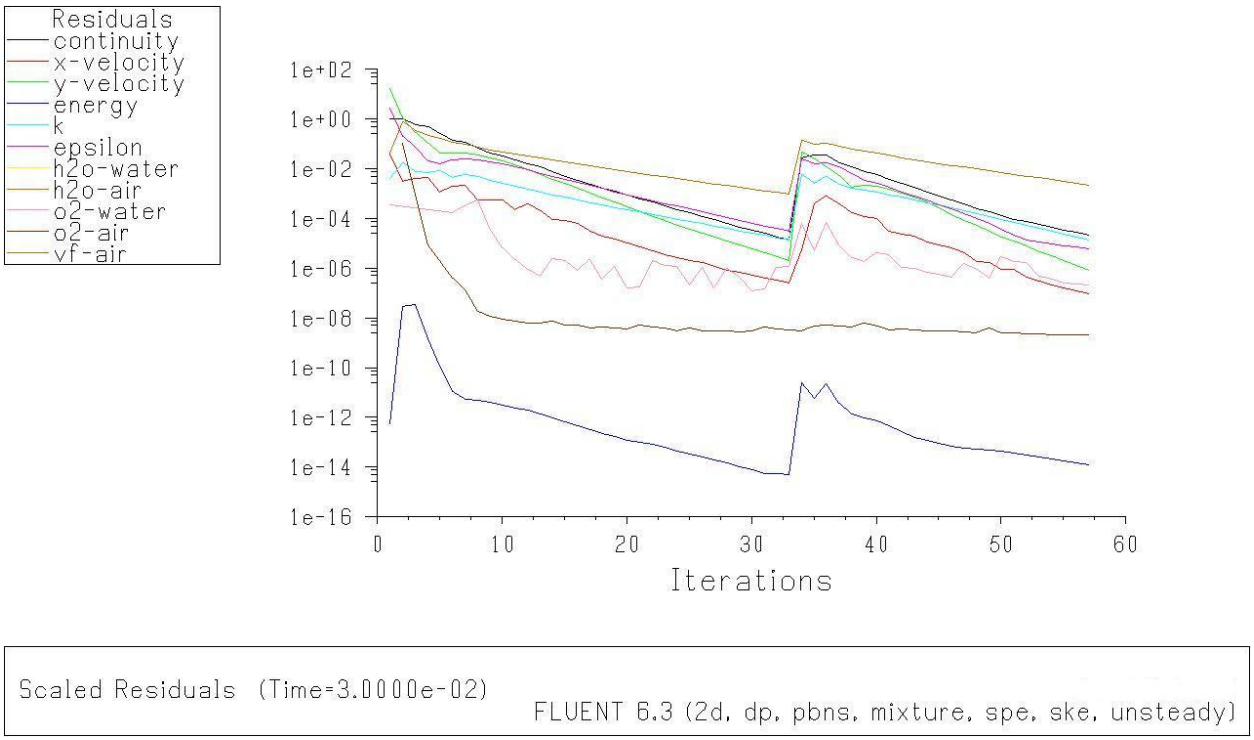

Fig. 3.3. Plot of residuals for k-epsilon solver method as the iterations proceeds

Convergence and accuracy is important during solution. A convergence criterion of 10^{-3} has been used in the present simulation. Simulation has been carried out for a longer physical flow time till the solution reaches a quasi-steady state. Once the fully developed quasi-steady state is reached the average quantities in terms of time, axial and radial direction have been calculated.

CHAPTER 4
RESULTS AND DISCUSSION

A gas-liquid bubble column of diameter 0.1m and height 1.88m has been simulated using commercial CFD software package FLUENT 6.3.26. The results obtained have been presented graphically in this section.

While simulating the column profile changes with time. But after some time no significant change in the profile is observed. This indicates that the column has come to a quasi steady state. Contours of mass fraction of O_2 in liquid with respect to time of gas-liquid interaction are shown in Fig. 4.1 with inlet air velocity 0.1 m/s and water 0.1 m/s. Simulation was carried out till there is no significant change in the oxygen concentration profile in water. Even though the oxygen concentration profile appears similar for 100 to 130 sec the simulation was continued for 150 sec.

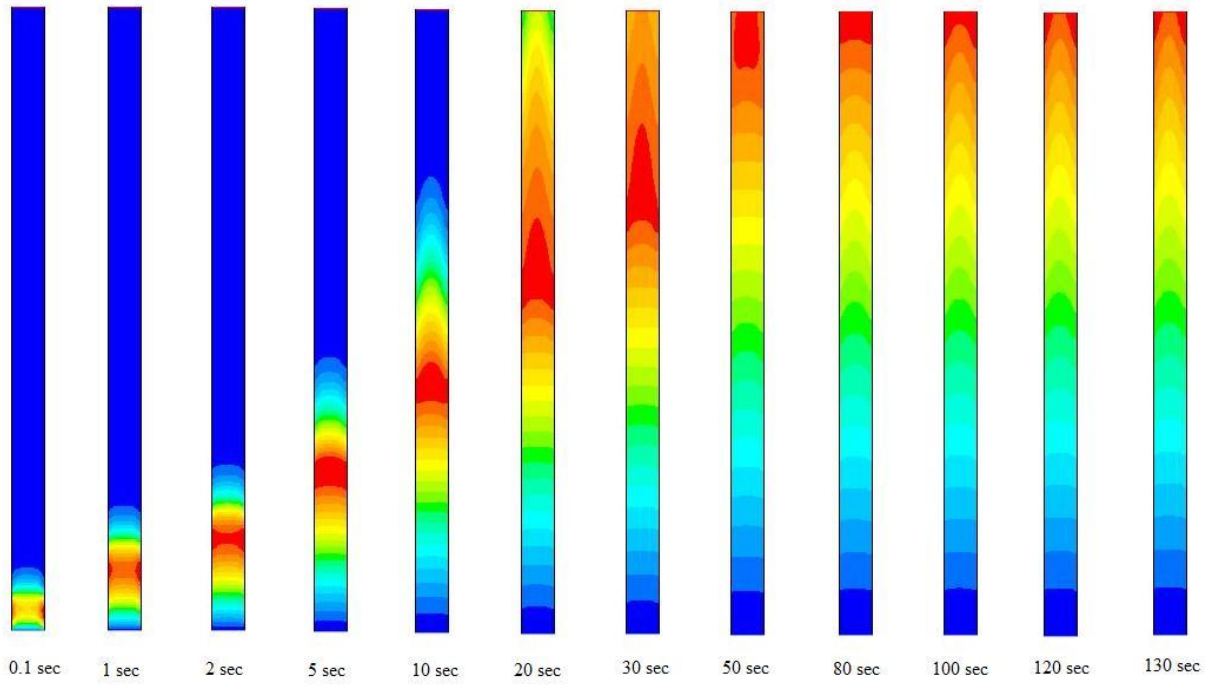

Fig. 4.1. Counters of mass fraction of Oxygen (O_2) in Water for water velocity of 0.1 m/s and air velocity of 0.1 m/s.

4.1 Phase Dynamics

Contours of volume fraction of liquid for water velocity of 0.1 m/s and air velocity of 0.1 m/s until quasi-steady state is reached is shown in Fig. 4.2.

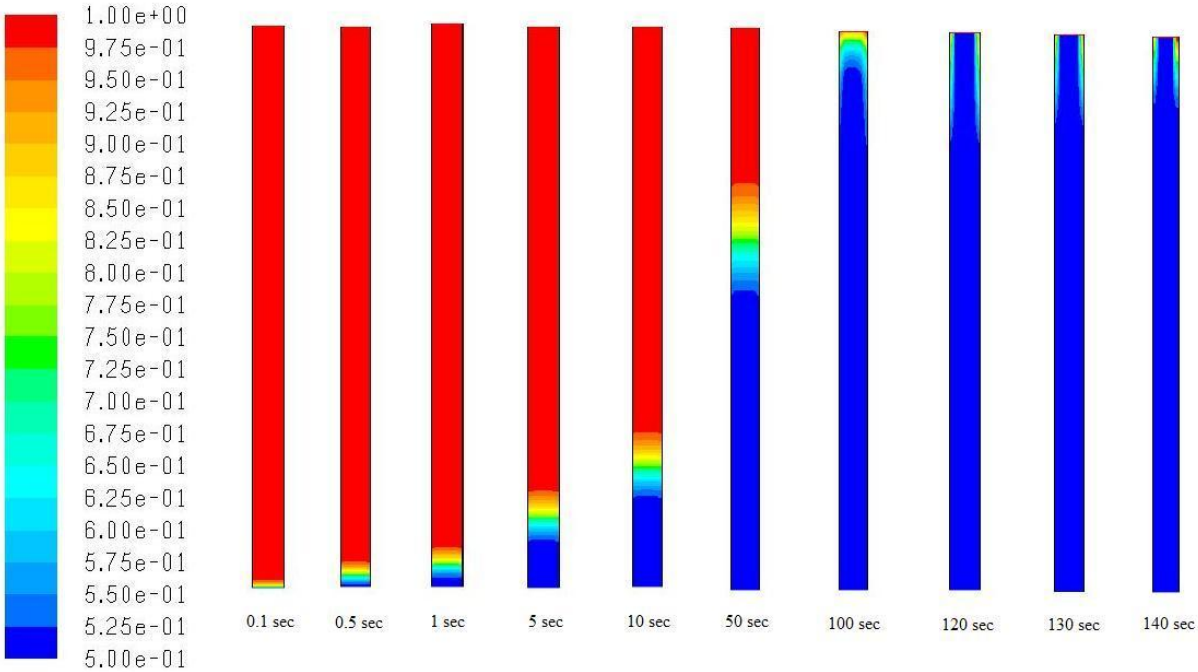

Fig. 4.2. Contours of volume fraction of liquid for water velocity of 0.1 m/s and air velocity of 0.1 m/s.

The volume fraction of liquid in the column is similar throughout the column for 120sec, 130 sec and 140 sec which indicates the bed has achieved the quasi-steady state.

Gas Holdup

Gas holdup is obtained as mean area-weighted average of volume fraction of air at sufficient number of points in the bubble column. As shown in the adjoining Fig. 4.2 volume fraction of air is almost the same at all points in the column. Hence area weighted average of volume fraction of air is determined at heights 10cm, 20 cm, 30 cm etc. When these values are averaged gives the overall gas holdup. Gas holdup plays a very important role in gas-liquid mass transfer. The rate of mass transfer depends on the gas holdup of the column. It is found that higher the gas holdup higher is the mass transfer rate of oxygen. Fig. 4.3 shows the variation of gas holdup with water velocity for a constant air velocity of 0.1 m/s. Figure indicates that the gas holdup decreases with increase in liquid velocity. It is clear from Fig. 4.4 that the gas holdup increases monotonically with increase in gas (air) velocity.

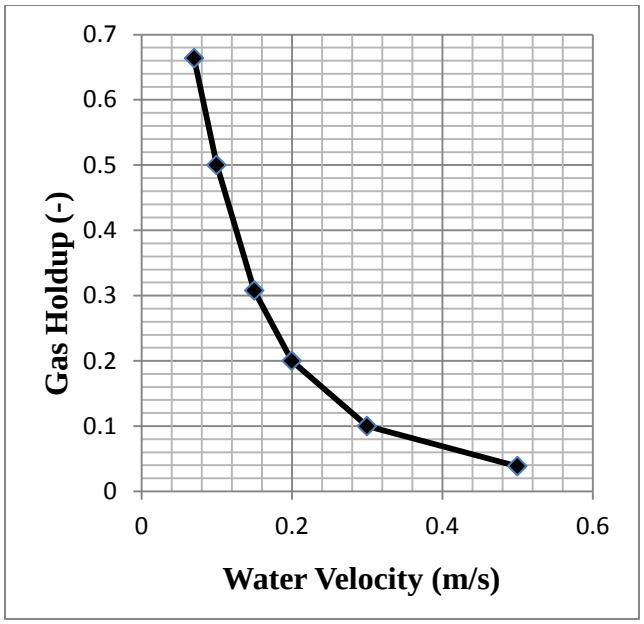

Fig. 4.3. Gas holdup vs. water velocity for constant air velocity of 0.1m/s.

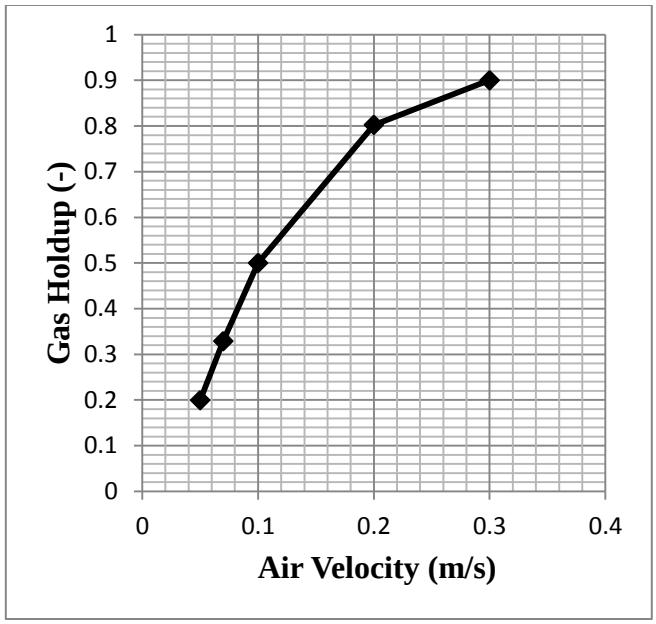

Fig. 4.4. Gas holdup vs. air velocity for constant liquid velocity of 0.1m/s.

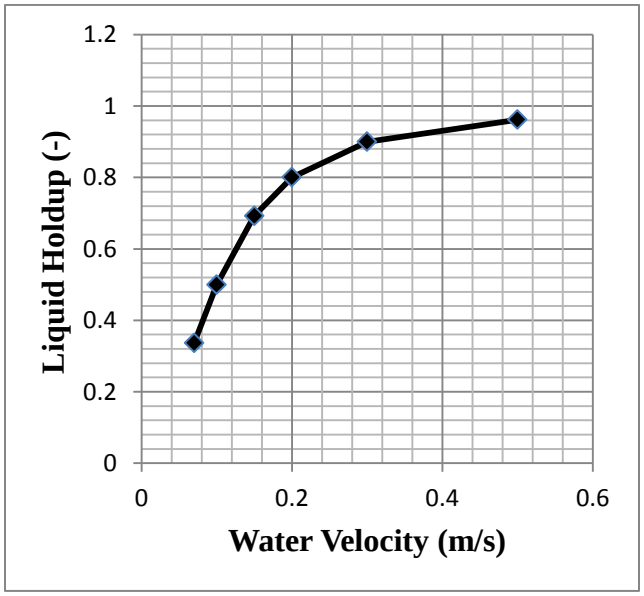

Fig. 4.5. Liquid holdup vs. water velocity for constant air velocity of 0.1m/s.

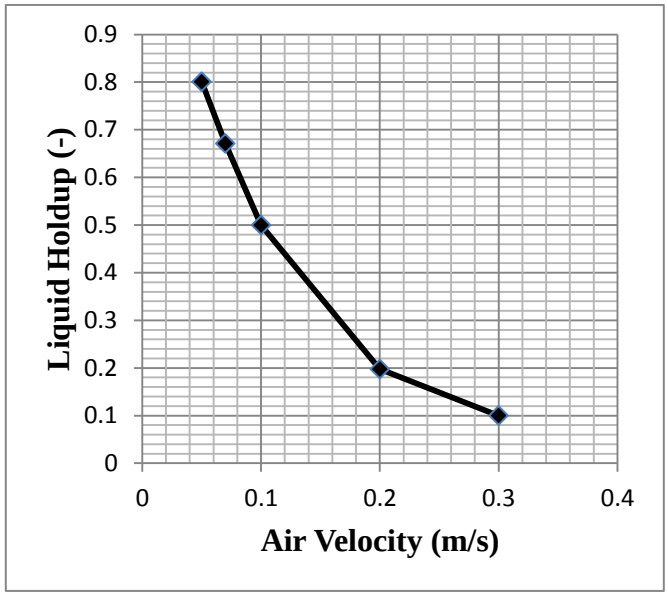

Fig. 4.6. Liquid holdup vs. water velocity for constant liquid velocity of 0.1m/s.

Liquid Holdup

Figs. 4.5 and 4.6 show the variation of liquid (water) holdup with inlet liquid and gas velocities respectively. It has been observed that with increase in liquid velocity, liquid holdup increases whereas with increase in gas velocity the liquid holdup decreases.

4.2 Liquid and gas velocities

In gas-liquid bubble column, the velocities of gas and liquid vary with time and location in the column. Vectors of velocity magnitude of water and air in the column obtained at inlet water velocity of 0.1m/s and inlet air velocity of 0.1m/s after the quasi steady state is achieved are shown in Figs. 4.7 and 4.8. These vectors show velocity magnitude with direction and thus are helpful in determining flow patterns in bubble column.

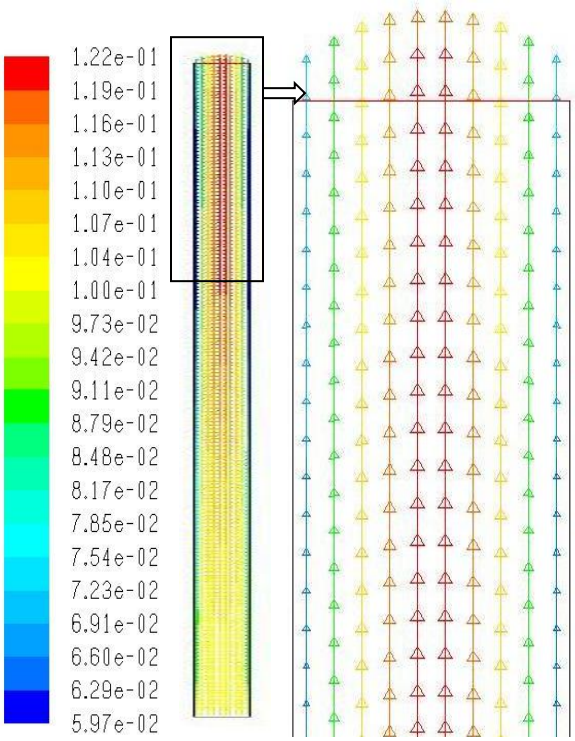

Fig. 4.7. Velocity vectors by velocity magnitude in liquid and the magnified view of the boxed part.

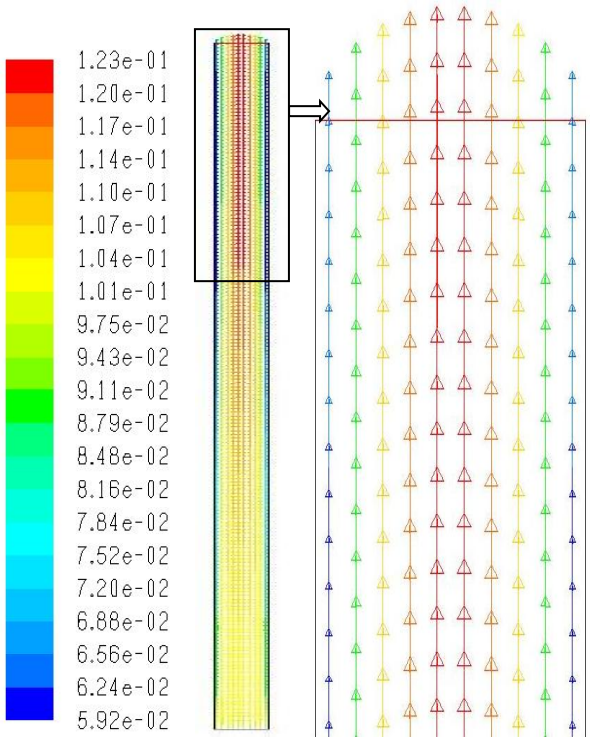

Fig. 4.8. Velocity vectors by velocity magnitude in air and the magnified view of the boxed part.

It can be seen from Fig. 4.7 that there is not much transition in liquid velocity in the column. The velocity varies from 0.100m/s at inlet to 0.122m/s at outlet. This can be explained by the fact that the radial transition in velocity is found to be greater in upper part than in lower part of the column. In lower part the velocity throughout the cross section remains almost equal. This is because it assumed that the liquid enters the column uniformly over the entire cross-section. As the liquid moves up the column it develops a parabolic profile. The velocity of the liquid at the wall is zero and is maximum at the center of the column.

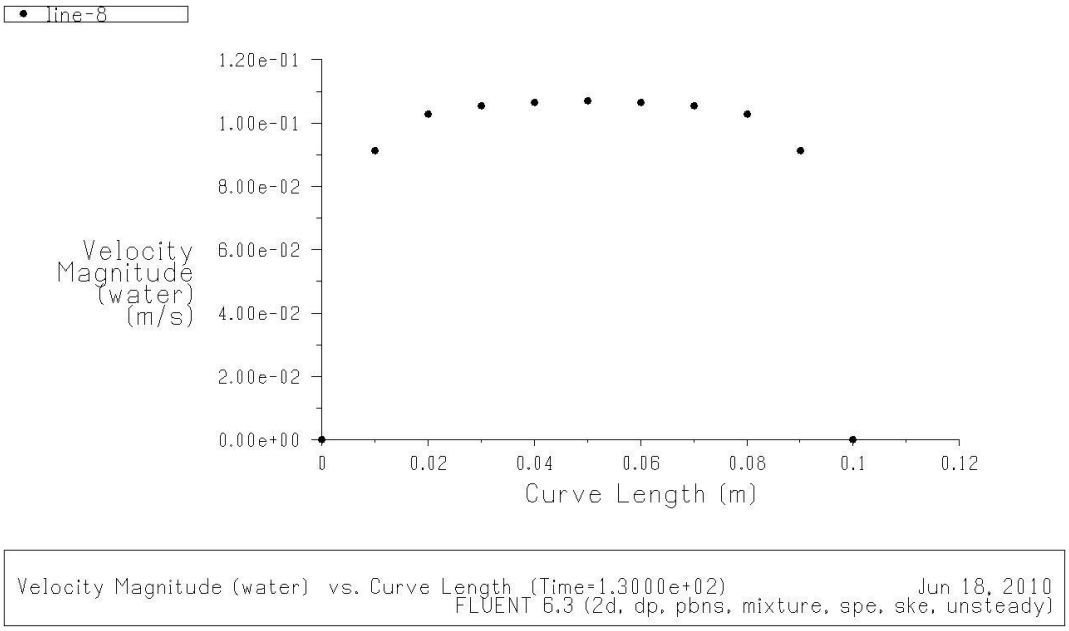

Fig. 4.9. XY plot of velocity profile of water across the cross section of column at height 0.5m.

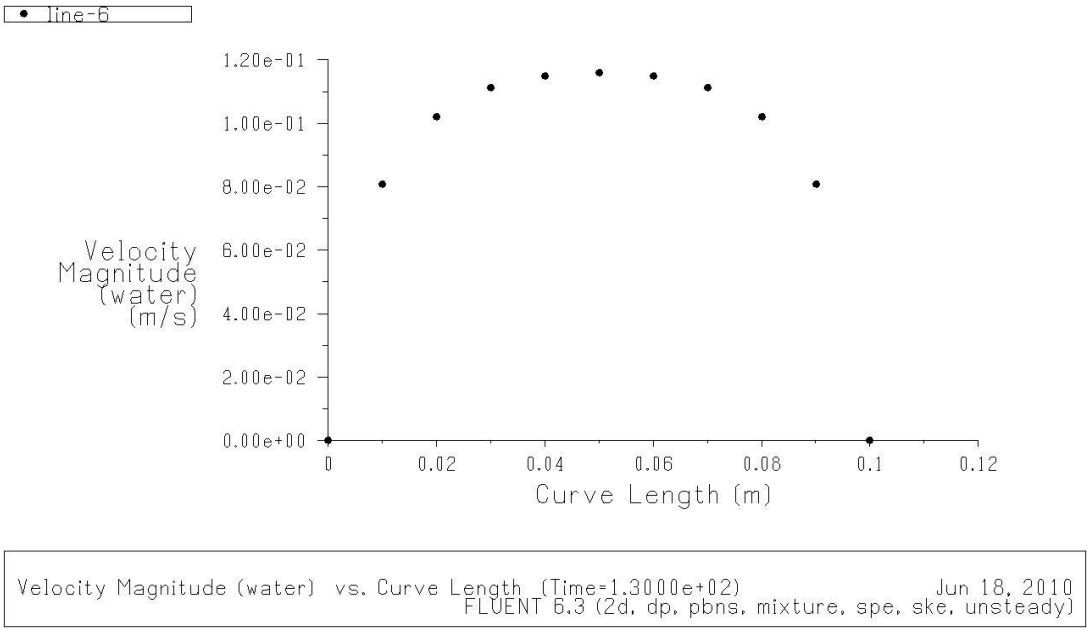

Fig. 4.10. XY plot of velocity profile of liquid across the cross section of column at height 1m.

The graphs shown in Figs. 4.9 - 4.11 show the velocity profile for water at different heights of the column. The profile is nearly uniform in the lower portion and there is considerable variation in top portion of the column. The curve length in the graph stands for diameter of the column.

The curves were defined at different heights along the cross-section of column and the graphs where plotted for velocity magnitude of water at quasi-steady state.

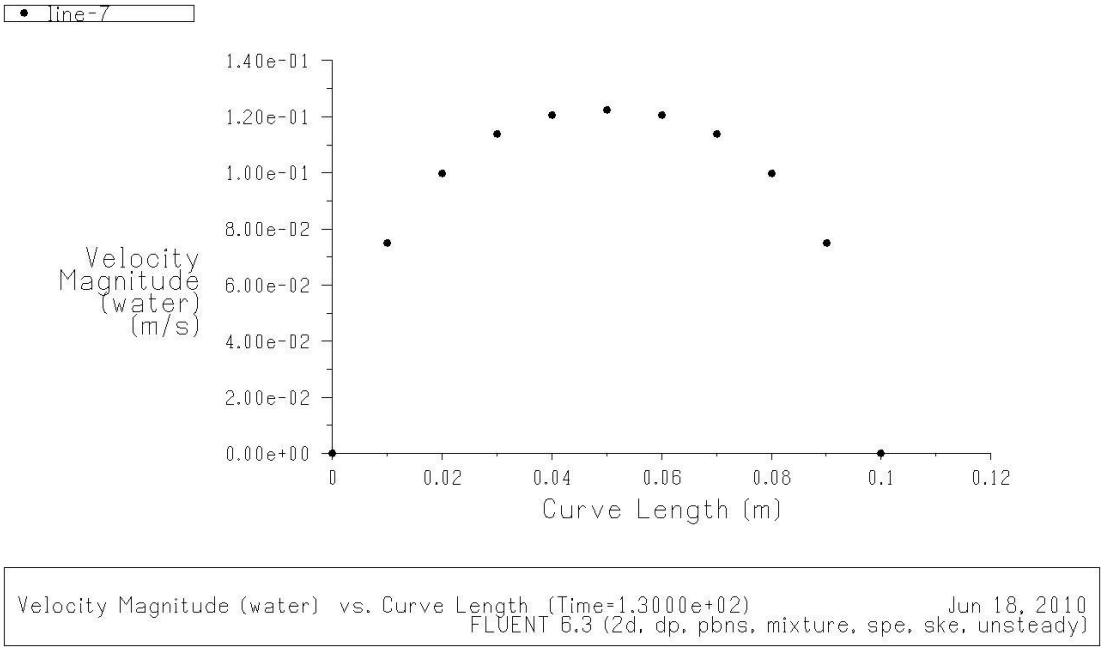

Fig. 4.11. XY plot of velocity profile of liquid across the cross section of column at height 1.5m.

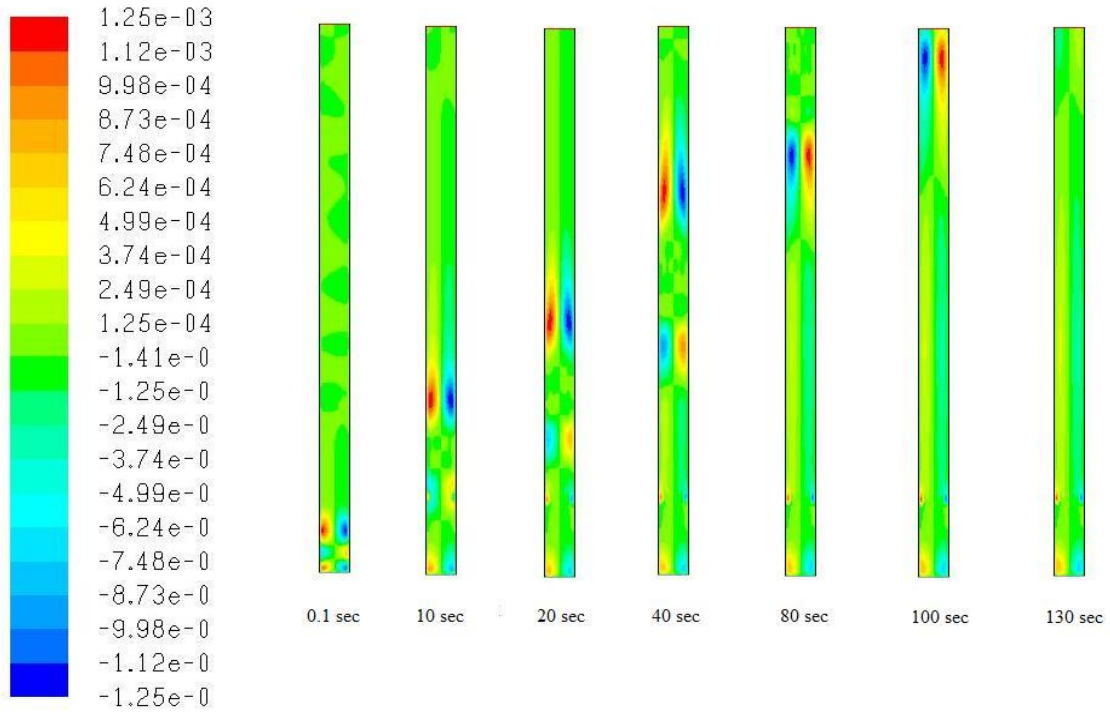

Fig. 4.12. Snapshots of radial velocity of air in the column at different time intervals.

The radial local velocity of air varies with time and space in the column. Fig. 4.12 displays the x-component of velocity magnitude of air at local points at different time intervals in the column. Fig. 4.13. displays the snapshots of axial velocity of air in the column at different locations and time intervals.

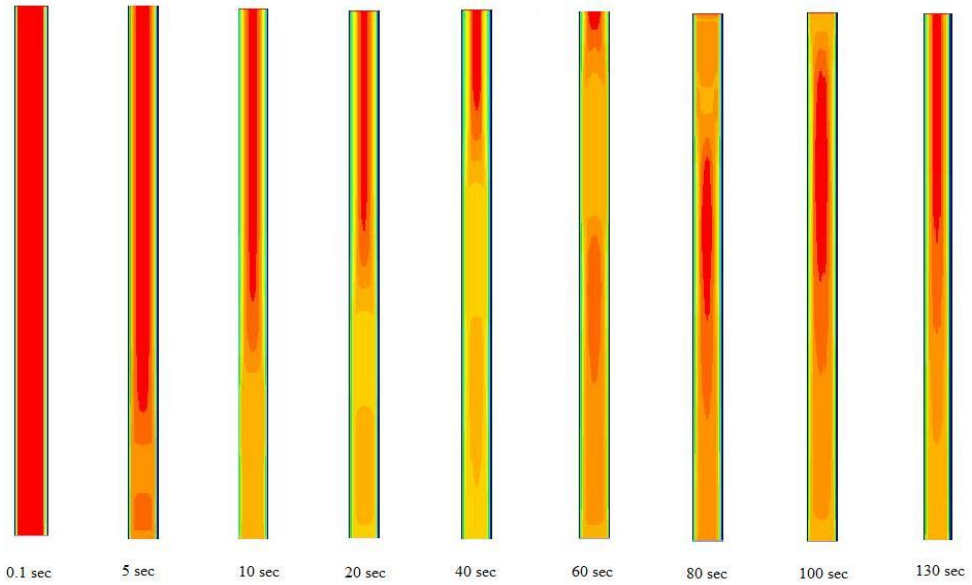

Fig. 4.13. Snapshots of axial velocity of air in the column at different time intervals.

4.3. Pressure Drop

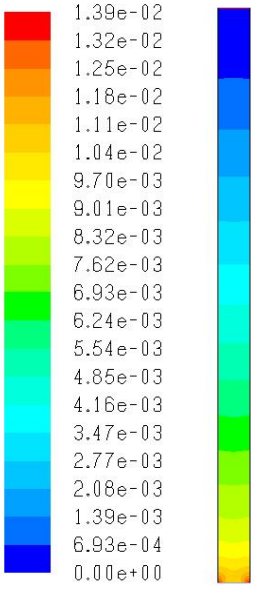

Fig. 4.14. Contours of static gauge pressure (mixture phase).

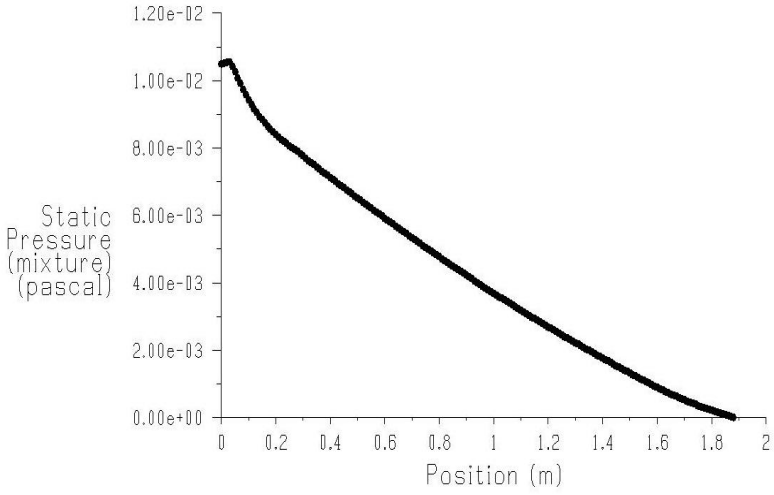

Fig. 4.15. XY graph of static pressure vs. column height.

Fig. 4.14 shows the contours of static gauge pressure (mixture phase) in the column obtained at water velocity of 0.1m/s and air velocity of 0.1m/s. The pressure at the bottom is high and at the top is low. Also pressure at inlet and outlet can be determined which is helpful in finding the pressure drop across the column. The XY plot (Fig. 4.15) shows the frictional pressure drop of the fluid flow along the column with the magnitude of the pressure drop is higher at the bottom.

4.4 Gas-Liquid Mass Transfer

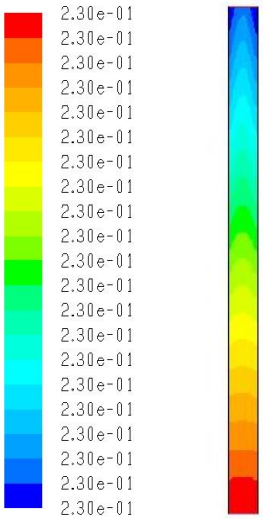

Fig. 4.16. Mass fraction profile of oxygen in air in the column.

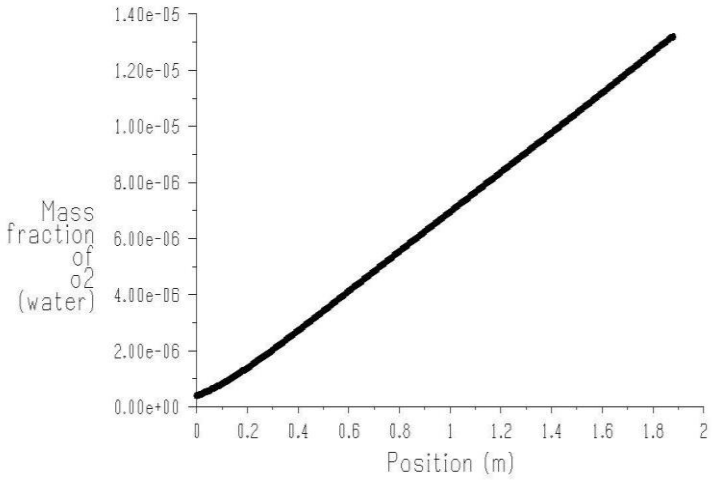

Fig. 4.17. XY Plot of liquid oxygen mass fraction vs. column height.

The concentration of oxygen in air is higher as it enters the column but as it passes through the column it loses its oxygen to oxygen depleted water until equilibrium is achieved between the two phases. Fig. 4.16 explains this clearly. The mass fraction of O_2 in water rises maximum to a value of 14 ppm from 0.4 ppm while that of O_2 in air drops from 0.23 to 0.229. It is clear from Fig. 4.17 that oxygen concentration in water gradually increases with the height of the column up to the equilibrium concentration is reached.

It can been seen from Fig. 4.18 that as the difference in the velocities of gas and the liquid increases the amount of mass transferred decreases i.e. as one of the fluid has a considerable inlet velocity the residence time for the fluid decreases and proper gas liquid interaction doesn't take place. Similar explanation can be applied to Fig. 4.19 over increase in mass transfer as the fluid velocity decreases.

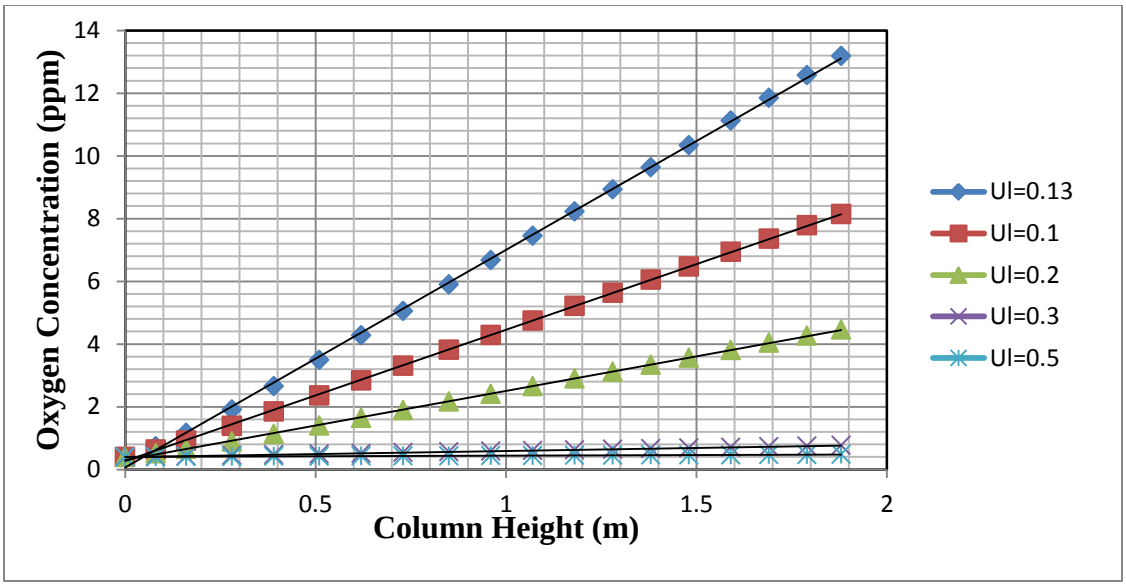

Fig. 4.18. Plot of variation in oxygen transferred to de-aerated water at constant air velocity of 0.1 m/s and various liquid velocities.

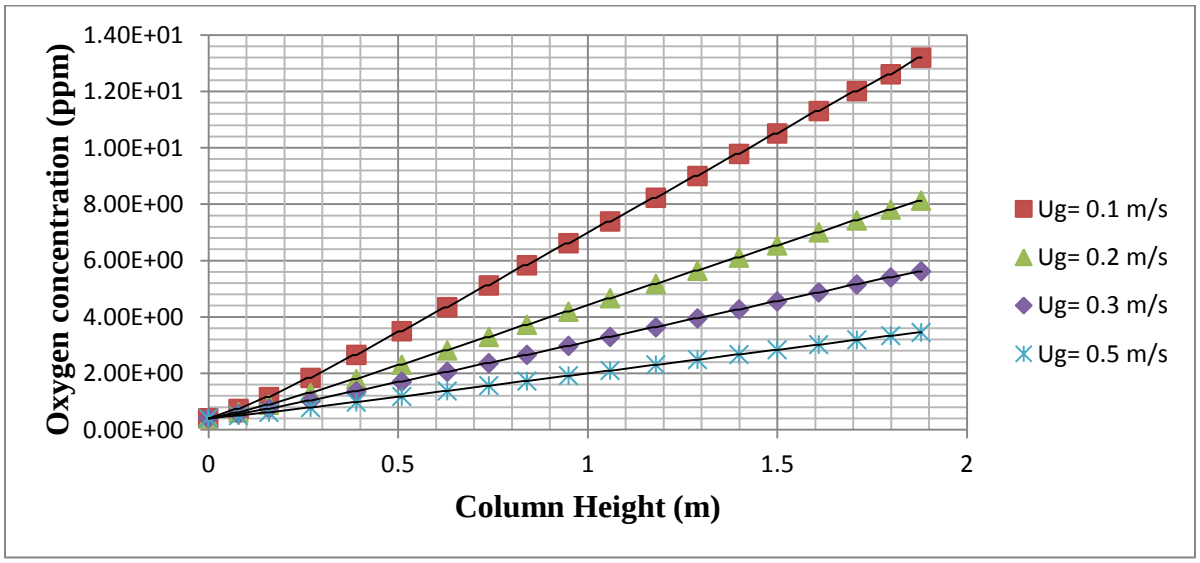

Fig. 4.19. Plot of variation in oxygen transferred to de-aerated water at constant liquid velocity of 0.1 m/s and various gas velocities.

For comparison experimental data was taken from the paper (Catros et al., 1975). A separate 2D coarse mesh was generated in gambit meeting the specifications of the column used. Column is 3.2 m high with internal diameter of 0.172 m. Mesh size was taken to be 0.01m. Mesh generated contained overall 5440 cells and 11217 faces.

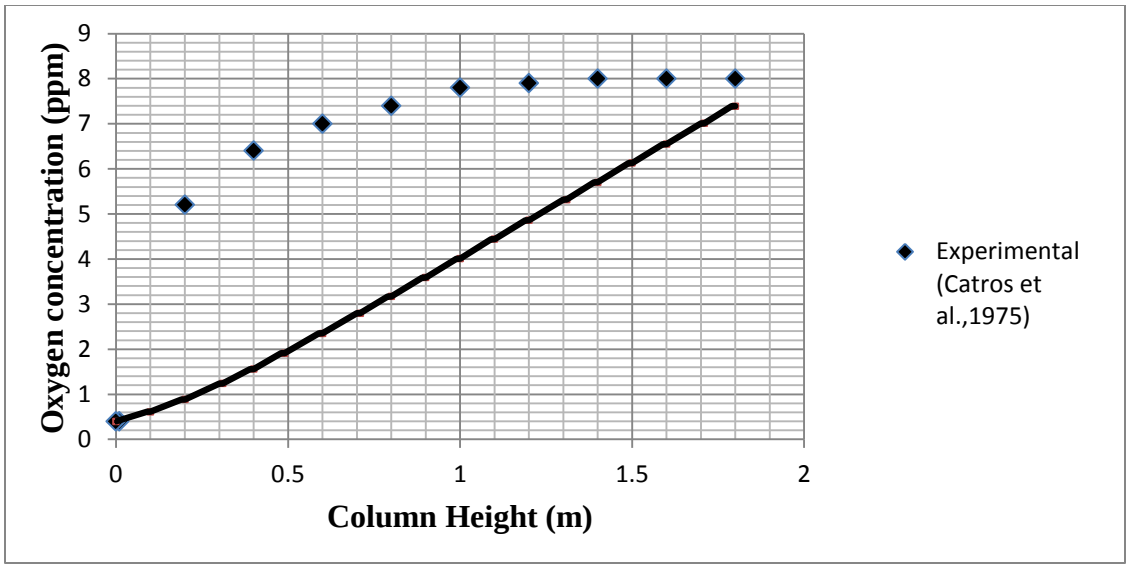

Fig. 4.20. Comparison graph between experimental and simulated results.

It is evident from Fig. 4.20 that the simulated results are found to be close to the experimental readings at a bed height of approximately 1.88 m but due to assumption of constant mass transfer rate the oxygen concentration in the liquid phase deviates a lot from the experimental one at the other positions. The deviation from the experimental results may also be due to some assumptions made in the discretization schemes.

CHAPTER 5
CONCLUSION

In the present investigation a co-current gas-liquid up-flow bubble column (10 cm ID and 1.88m height) has been simulated using Fluent. The various parameter studied include bed dynamics such as phase holdups, pressure drop, velocity profile and gas-liquid mass transfer. The eulerian-eulerian approach with mixture multiphase model and segregated solver has been used. The standard k-ε model has been used to model turbulence. The species model has been used to simulate the oxygen transfer from gas to liquid as species in the two phases. The simulated results have been presented graphically in chapter 4 results and discussion in detail.

The gas holdup has been found to increase with increase in gas velocity but decreases with increase in liquid velocity. A similar trend has been observed for the liquid phase with the corresponding phase velocities. The gas holdup has been found to vary from 0.2 to 0.9 for gas velocity range of 0.05 to 0.3 and constant liquid velocity of 0.1 m/s. It has been observed that the local gas velocity depends on the physical flow time. The averaged values of the gas and the liquid velocities have been found to be a maximum of 0.122m/s at the center of the column. The velocity profiles for both the phases are parabolic for a fully developed flow. A maximum gas velocity of 0.123 m/s and maximum liquid velocity of 0.122 m/s is observed for uniform fluid velocity of 0.1 m/s for each of the gas and liquid. A negligible frictional pressure drop of 0.0105 Pa has been observed for the gas liquid flow in the column.

It was found that the aeration depends strongly on the gas–liquid interfacial area, and therefore gas–liquid mass transfer dominates. The initial mass fraction of oxygen in water and the inlet air velocity had a significant effect on the overall mass transfer rate. The mass fraction of oxygen in water rises maximum to a value of 14 ppm from 0.4 ppm while that of oxygen in air drops from 0.23 to 0.229 for uniform liquid and air velocity of 0.1 m/s. The steady state oxygen concentration in water has been found to decrease drastically from 13 ppm to a little above 0.4 ppm for the liquid velocity ranging from 0.1m/s to 0.5m/s and a constant gas velocity of 0.1m/s. The laminar diffusion coefficient has been found to be uniform throughout the column and its value is $2.88e^{-5}$ m^2/sec. The difference between the simulated and the experimental results may be due to certain assumptions made during the simulation such as the constant rate mass transfer.

REFERENCES

Arcuri, E.J., Slaff, G., Greasham R., 1986. Continuous production of thienamycin in immobilized cell systems. Biotechnology Bioengineering. 28, 842– 849.

Blažej, M., Cartland, G. M., Generalis, S. C., Markoš, J., 2004. Gas–liquid simulation of an airlift bubble column reactor. Chemical Engineering and Processing. 43, 137–144.

Bordonaro, J. L., Curtis, W. R., 2000. Inhibitory role of root hairs on transport within root culture bioreactors. *Biotechnology* and *Bioengineering* 70, 176–186.

Catros, A., Bernard, J.R., 1975.Generalized Model for Gas-Liquid Mass Transfer in Three-Phase Fluidized. Powder Technology 44, 159-168.

Cockx, A., Do-Quang, Z., Audic, J.M., Line,A. Roustan, M., 2001. Global and local mass transfer coefficients in waste water treatment process by computational fluid dynamics. Chemical Engineering and Processing, 40, 187–194.

Deen, N.G., Solberg, T., Hjertager, B.H., 2001. Large eddy simulation of gas–liquid flow in a square cross-sectioned bubble column. Chemical Engineering Science. 56, 6341–6349.

Degaleesan, S., Dudukovic, M., Pan, Y., 2001. Experimental Study of Gas-Induced Liquid-Flow Structures in Bubble Columns. AIChE Journal 47, 1913-1931.

Duran, E., Taghipour, F., Mohsen, M., 2009. CFD modeling of mass transfer in annular reactors. International Journal of Heat and Mass Transfer, 52, 5390–5401.

Ekambara, K., Dhotre, M., Joshi, J.B., 2005. CFD simulations of bubble column reactors: 1D, 2D and 3D approach. Chemical Engineering Science, 60, 6733 – 6746.

Fayollea, Y., Cockx, A., Gillot, S., Roustan, M., Héduit A., 2007. Oxygen transfer prediction in aeration tanks using CFD. Chemical Engineering Science 62, 7163–7171.

Fluent 6.3 Documentation, 2006. Fluent Inc., Lebanon.

Gimbun, J., Rielly, C. D., Nagy, Z. K., 2009. Modelling of Mass Transfer in Gas-Liquid Stirred Tanks Agitated by Rushton Turbine and CD-6 Impeller. 13th European Conference on Mixing. London.

Han, L., Al-Dahhan, M. H., 2007. Gas–liquid mass transfer in a high pressure bubble column reactor with different sparger designs. Chemical Engineering Science. 62, 131–139.

Haroun, Y., Legendre, D., Raynal, L., 2010. Volume of fluid method for interfacial reactive mass transfer: Application to stable liquid film. Chemical Engineering Science. doi:10.1016/j.ces.2010.01.012.

Joshi, J.B., 2001. Computational Flow modelling and design of bubble column reactors. Chemical Engineering Science, 56, 5893–5933.

Kumar, A., 2009. CFD Modeling of Gas-Liquid-Solid Fluidized Bed. B.Tech. Thesis, NIT,Rourkela, India.

Kantarci, N., Borak, F., Ulgen, K. O., 2005. Bubble column reactors (Review). Process Biochemistry. 40, 2263–2283.

Kerdouss, F., Bannari, A., Proulx, P., Bannari, R., Skrga, M., Labrecque, Y., 2008. Two-phase mass transfer coefficient prediction in stirred vessel with a CFD model. Computers and Chemical Engineering. 32, 1943–1955.

Lohse, M., Alper, E., Deckwer, W.D., 1983. Modeling of batch catalytic chlorination of toluene in a bubble column. Chemical Engineering Science 38, 1399-1409.

Lopes, R.J.G., Quinta-Ferreira, R.M., 2007. Multiphase CFD Modeling of Trickle-Bed Reactor Hydrodynamics. Proceedings of the World Congress on Engineering and Computer Science (WCECS 2007). San Francisco, USA.

Mohapatra, D., Rakh, K., 2007. CFD Modeling of Multi-phase Fluidized Bed. B. Tech. Thesis, NIT, Rourkela, India.

Moilanen, P., 2009. Modeling gas liquid flow and local mass transfer in stirred tanks. Chemical Engineering Report Series Espoo. Helsinki University of Technology, Helsinki.

Mousavi, S.M., Jafari, A., Yaghmaei, A., Vossoughi, A., Turunen, I., 2007. Proceedings of the World Congress on Engineering and Computer Science (WCECS 2007), San Francisco, USA.

Mousavi, S.M., Jafari, A., Yaghmaei, S., Vossoughi, M., Turunen I., 2008. Experiments and CFD simulation of ferrous biooxidation in a bubble column bioreactor. Computers and Chemical Engineering. 32, 1681–1688.

Mousavi, S.M., Jafari, A., Chegini, S., Turunen, I, 2009. CFD simulation of mass transfer and flow behavior around a single particle in bioleaching process. Process Biochemistry, 44, 696–703.

Ogbonna, J.C., Mashima, H., Tanaka, H., 2001. Scale up of fuel production from sugar beet juice using loofa sponge immobilized bioreactor. Bioresource Technology. 76, 1–8.

Pandey, S., 2010. CFD Simulation of Hydrodynamics of Three-phase Fluidized Bed. M.Tech. Thesis. NIT, Rourkela, India.

Pfleger, D., Gomos, S., Gilbert, N., Wagner, H. G., 1999. Hydrodynamic simulation of laboratory scale bubble columns: fundamental studies of Eulerian–Eulerian modeling approach. Chemical Engineering Science, 54, 5091–5099.

Prakash, A., Margaritis, A., Li, H., Bergougnou, M.A., 2001. Hydrodynamics and local heat transfer measurements in a bubble column with suspension of yeast. Biochemical Engineering Journal, 9, 155–163.

Sokolichin, A., Eigenberger, G., Lapin, A., Lübbert, A., 1997. Dynamic numerical simulation of gas–liquid two-phase flows: Euler–Euler versus Euler–Lagrange. Chemical Engineering Science, **52**, 611–626.

Sun, Y., Furusaki, S., 1990. Effects of product inhibition on continuous acetic acid production by immobilized Acetobacteraceti: theoretical calculations. Journal of Ferment Bioengineering. 70, 196–198.

Tabib, M. V., Roy S. A. Joshi, J. B., 2008. CFD simulation of bubble column—An analysis of interphase forces and turbulence models. Chemical Engineering Journal, 139, 589–614.

Zhang, D., 2007. Eulerian modeling of reactive gas-liquid flow in a bubble column. PhD Thesis. Universiteit Twente, Enschede, the Netherlands.